Shock-induced combustion of aluminum particle clusters investigated with resolved sharp-interface two-dimensional simulations

Pratik Das and H. S. Udaykumar

Phys. Rev. Fluids **6**, 083201 — Published 30 August 2021

DOI: 10.1103/PhysRevFluids.6.083201

Shock-induced combustion of aluminum particle clusters investigated with resolved sharp-interface two-dimensional simulations

Pratik Das and H. S. Udaykumar

Department of Mechanical Engineering, The University of Iowa, Iowa City, IA-52242, USA

Abstract

The vaporization and combustion of clusters of aluminum particles in shocked flows is studied through interface-resolved 2D numerical simulations. These meso-scale simulations elucidate, for the first time, aspects of vaporization and burning in molten aluminum(Al) particle clusters that are markedly different from an isolated burning Al particle. Unsteadiness due to shock-generated baroclinic vorticity (inviscid mechanisms) and interactions between the wakes of molten Al particles (viscous mechanisms) are found to have significant effects; vortical mixing facilitates kinetically-limited combustion of the particles located upstream in the cluster. Whereas, for particles located downstream in the cluster, the interaction with the low-speed, oxygen-lean wake of the upstream particles leads to diffusion-limited combustion. Results show that particles in a cluster have lower rates of vaporization and combustion than isolated particles under the same overall flow conditions. To isolate inviscid and viscous effects, the flame structure and vaporization rate for particles in a cluster are quantified in terms of local flow conditions, i.e. the local Mach number, Reynolds number, location of a particle in the cluster, and volume fraction. The results obtained in this study will be useful in understanding and modelling the meso-scale physics of shock-induced burning of explosively dispersed reactive aluminum particles.

Keywords: Aluminum combustion, particle combustion, shock particle interaction, sharp interface methods

1. Introduction

The rapid energy released during the combustion of high-speed multiphase mixtures, e.g. micron-scale particles of Aluminum(Al) or other metal additives in air or deflagration/detonation products is of relevance to many emerging civil and military applications [1,2]. The enthalpy of combustion of Al particles is 5-6 times higher than that of the non-metallic energetic compounds (e.g. Ammonium perchlorate, TNT, RDX, HMX, etc.) [1,3]. Al particles are therefore extensively used as energetic additives [4–6] in propellants and explosives. During combustion of the aluminized energetic materials, the Al particles first undergo a phase change from solid to liquid. An oxide layer forms rapidly around the liquid Al particles; this layer subsequently cracks open and the resulting molten Al burns in the surrounding oxidizer, thereby enhancing the performance of energetic materials.

The rate of energy released by the combustion of the Al particles depends on the combustion dynamics (e.g. shock interactions, vaporization rates, flame structures) in the surrounding high-speed gas flow. While the combustion of individual Al particles in hot, high-speed reacting flows has been studied through experiments and simulations, the combustion behaviour of *Al* particles clusters at the length scale of the particles (i.e. the meso-scale) is not yet well understood. This work fills this knowledge gap by studying for the first time the detailed meso-scale physics of combustion of *Al* particle clusters in high Mach number flows. Combustion of Al particle clusters in shocked flows is studied through interface-resolved 2D numerical simulations. The flow conditions in current simulations are characterized using the Mach number(M_s), Reynolds number(Re_D) and particle volume fraction in percentage(ϕ) as defined below:

$$M_s = \frac{u_s}{c_{us}} \tag{1}$$

$$Re_D = \frac{\rho_{ps} u_{ps} D}{\mu} \tag{2}$$

$$\phi = \frac{25 n \pi D^2}{A_c} \tag{3}$$

where u_s is the speed of the shock in the laboratory frame of reference and c_{us} is the speed of sound in the unshocked air. ρ_{ps} and u_{ps} are the post-shock density and velocity of air in the laboratory frame of reference. μ is the viscosity of air, D is the initial diameter of the particles in a cluster. n and A_c are the total number of particles and the area covered by the cluster in 2D simulation. The present high-resolution, sharp interface numerical simulations provide new insights into the effects of local flow conditions, on the combustion behavior of the Al particles in a cluster, distinguishing the physics in a cluster from that of an isolated particle.

1.1 State-of-the-art of modelling of combustion of Al particles

The combustion of isolated Al particles has to date been fairly well studied through experiments [7–10]. A comprehensive review of the earlier experimental efforts on developing correlations for the burning time of *Al* particles and particles can be found in [7]. More recently, spectroscopy [11], pyrometry [12], and other advanced optical imaging methods [13] have been used to understand the combustion of Al particles and particles. These previous studies have advanced the threshold of our understanding of the combustion of Al particles in the dilute regime, where reacting Al particles are sufficiently far apart that they can be treated as isolated particles. Such flow scenarios generally occur in the combustion chamber of solid rocket motors. However, the dilute flow assumption does not hold during the detonation of aluminized high explosives or near the surfaces of aluminized propellants, where a higher volume fraction of Al particles prevails($\phi \sim 10\% - 30\%$) [14]. In a cluster of Al particles at higher volume fractions, the interaction between the dispersed particles influences their ignition and combustion [15–18].

The current body of knowledge--experimental as well as theoretical-- on vaporization and burning of particle clusters is rather sparse. Shock-induced combustion of Al particle and particle clouds has been investigated experimentally [1,4,17,18]. Boiko et al. [17–19] studied the effects of pressure, particle diameter, and volume fraction on the ignition characteristics of Al particles clouds in shocked flows. The effects of particle diameter on the cumulative burning rate of Al particles clouds in post-detonation flow was investigated by Tanguay et al. [1]. Zhang et al. [4,20] showed that the detonation characteristics of the Al particle clouds suspended in air depends on the initial pressure. These previous experimental studies were focused on determining the macro-scale properties of Al particle combustion such as the effects of particle size, volume fraction and initial flow conditions on the ignition delay, burning rate and characteristics of detonation waves. However, the underlying meso-scale physics at the length scale of the particles governing the macro-scale combustion behaviour was not investigated in the above-mentioned studies.

Studying the particle-resolved meso-scale physics of *Al* particle combustion in shocked flows through experiments is expensive and challenging. It is difficult to create the high-pressure and high-speed conditions observed during explosions in a controlled laboratory environment [5]. Additionally, observing and measuring the combustion of an *Al* particle of few micrometers in diameter over a duration of a few microseconds becomes a daunting task even with modern laboratory equipment, although some preliminary efforts are being undertaken [21,22]. Numerical modelling [23–26] offers an alternative route for studying *Al* particle combustion in the shocked flows. Several numerical models for the combustion of Al particle clouds under post-detonation conditions have been developed [1,4,16,27,28]. In such multiphase models, the continuous gaseous phase is modelled in an Eulerian frame of reference, while the dispersed Al particles can be modeled either as one phase in a continuous multi-phase mixture in the Eulerian frame of reference [16,29,30] or as point particles in the Lagrangian frame of reference [28,31,32]. In such multiphase models, the interaction of the carrier flow with the particles is modeled using closure terms (empirical correlations) in the governing equations. The detailed meso-scale interactions of the post-detonation flow with the individual particles in a cluster are not resolved in these studies.

1.2 Understanding the physics of combustion in particle clusters

Interface-resolved numerical models for the combustion of isolated Al particles in low subsonic flows were developed in [23,24,33,34], while numerical models of aluminum particle combustion in high-speed flows have been published only recently by Houim et al. [35] and Das et al. [26,36,37]. These previous models considered the combustion of isolated Al particles only. To the authors' knowledge the current paper is the first attempt at modelling the combustion of Al particle clusters in shocked flows to study the interaction of the reacting particles in high volume-fraction air-Al mixtures.

There is a limited understanding of the thermophysics of particle clusters in high-speed flows. The combustion behaviour of particles in high-speed flows can be characterized either as diffusion-limited or kinetically-limited [1,11,38]. Macro-scale models for the burn rate of Al particles under the assumption of kinetically-limited combustion are significantly different from the models for burn rate under the assumption of diffusion-limited combustion [1]. For instance, a "wake flame" [39,40] characterizes kinetically-limited combustion of a particle while an "envelope flame" [39,40] indicates that the combustion is diffusion-limited [41]. However, it is challenging to observe the meso-scale flame structure of particles burning in shocked flows in experimental studies; the implications of flame structure can only be surmised based on the experimental measurements of the cumulative burn time data. The experimental measurements of Tanguay et al. [1] indicated that the Al particles in a cloud undergo kinetically-limited combustion in a post-detonation flow. On the other hand, Zhang et al. [4] proposed a surface kinetic oxidation and diffusion hybrid model to represent the burn rate of Al particles clouds in post-detonation conditions based on their pressure measurements in a detonation tube. An appropriate burn rate model must be used in a macro-scale calculation of Al particle combustion in shocked flow based on combustion behavior of particles under local conditions of M_s and Re_D within a particle cluster. However, the meso-scale flame structure and vaporization rates of an Al particle in a cluster over a range of M_s and Re_D remains poorly understood.

Previous experimental studies [15,18] show that the ignition and combustion of the Al particles and particles depend on the volume fraction ϕ in a cluster. Cassel et al. [15] showed that the flame-structure in a cluster of particles changes with ϕ. The effect of local ϕ on the flame-structure in a reacting particle cluster was also previously discussed in macro-scale multiphase calculations [16,42]. However, the existing models for the burn rate of Al particles in shocked flows [4,18,43,44] do not account for the clustering of particles i.e. they do not incorporate the dependence on ϕ. The meso-scale physics responsible for changes in the flame-structure and vaporization rate of particles with varying ϕ remains unexplored. In addition, the combustion behavior of Al particle clusters in shocked flows at different M_s and Re_D needs to be characterized to develop burn models for use in macro-scale multiphase models [16,28].

Interface-resolved direct numerical simulations(DNS) can address these gaps in current knowledge on Al particle cluster combustion in shocked flows. However, DNS of combustion of Al particles cluster in shocked flows is computationally expensive. Previously, such calculations have only been performed for hydrocarbon fuel droplets in low Mach number flows by a handful of researchers [45–47]. DNS of vaporization of a single droplet in shocked flows has been performed before [36]. However, such calculations for reacting clusters of droplets will be prohibitively expensive(leading to a mesh size of the order of billion grid points) and have not been performed yet. Two-dimensional interface-resolved simulations of reacting *Al* particle clusters are performed in this work to keep the computational costs tractable. The flame dynamics around particles primarily depend on the volatility of the molten particle(or vaporization mass flux), mixing of the vapor produced at particle surface with oxidizer in the free-stream through convective and diffusive transport, and the chemical kinetics of combustion of aluminum vapor in oxidizer. The 2D assumption in the current calculation will affect the process of mixing in the flow. However, the current 2D calculations serve to demonstrate the fundamental effects of shock-induced unsteadiness and interaction between particles on the combustion in a cluster.

During the combustion of an Al particle in the air, the aluminum oxide(Al_2O_3) layer around the particle cracks open [13] as it undergoes phase change. The molten oxide at the particle surface coalesces to form a small oxide-cap because of the difference in the surface tension of the liquid Al and Al_2O_3. As a result, the molten Al core of the particle is exposed to the air [48]. During the early stage of combustion, the oxide cap covers a small fraction of the surface area of the particle [49]. However, as the combustion of the particle approaches completion, the oxide cap grows in size due to the re-condensation of the gaseous oxide produced during combustion. The current study focuses on the combustion of the Al particles in the early stages after ignition. The rupture of the oxide layer and the re-condensation of the oxide are not considered because of the lack of current understanding of the physics of cap formation, its properties and its evolution. The combustion of molten pure Al particles is modelled using a levelset [50] based sharp-interface method for computing droplet combustion under the influence of shocks [26,36]. The reaction of vapor released from molten pure aluminum particles is studied in this work. The numerical results for the combustion of Al particle clusters are compared with isolated particles to study the effects of particle interaction on the flame structure and burning rate of the particles. Numerical calculations are performed for different ϕ, M_s, and Re_D to understand the role of local flow conditions in determining the combustion behavior of Al particle clusters at the meso-scale.

The rest of the paper is organized as follows: the numerical model for Al particle combustion is described in Section 2 and validation exercises are presented. Combustion of *Al* particle cluster at $M_s = 3.5, Re_D = 1000$ and $\phi = 20\%$ is studied and compared with the combustion of an isolated particle in section 3.1. Thereafter, the effects of $\phi, M_s$and Re_D on the combustion of Al particle, clusters are studied through DNS in sections 3.2, 3.3, and 3.4 respectively. Conclusions from the current study are presented in Section 4.

2. Methods

A Cartesian grid-based sharp-interface Eulerian method [51–53] is used to compute the combustion of the *Al* particle cluster under the influence of shocks. In this framework, the liquid and the gaseous phases in the computation domain are separated by a sharply defined interface. The governing equations for

reacting compressible flows are solved separately in each phase to evolve the flow-field in time. The levelset method [54] is used to track the liquid-gas interface embedded in the Cartesian grid. A modified Riemann solver based ghost fluid method (rGFM) [36] is used to impose the appropriate jump conditions (i.e. the conservations laws) at a sharply-defined reacting interface between the gas and the liquid Al particles. The phase-change at the sharp gas-liquid interface is modelled using the Schage-Knudsen equation [55]. A multistep Arrhenius kinetics model for combustion of Al particles in air given by Huang et al. [56] is used to compute the reaction in the gas-phase. The current numerical framework for computing the combustion of liquid Al particles was described in a series of previously published papers [26,36,37] and are not reproduced here in the interest of brevity. The numerical framework is presented in the supplementary material for completeness [57].

2.1 Calculation of the quantities of interest

The combustion of *Al* particle clusters under the influence of incoming shocks at various Mach numbers(M_s), Reynolds numbers(Re_D) and particle volume fractions(ϕ) is numerically studied using the sharp-interface framework. The post-shock conditions are selected as the reference conditions to define the nondimensional parameters characterizing the flow field and the quantities of interest such as the Reynolds number(Re_D), drag-coefficients(C_D), and Sherwood number(Sh). In the current calculations, particle clusters of uniform initial diameter(D) are considered and D is selected such that the desired Re_D is achieved for a given M_s.
The drag-coefficient of the i^{th} particle in the cluster is calculated from:

$$C_{D,i}(t) = \frac{F_{D,i}(t)}{0.5\rho_{ps}u_{ps}^2 D} \tag{4}$$

$F_{D,i}(t)$ is the x-component of the resultant force acting on the i^{th} particle in the cluster at time t.

The instantaneous Sherwood number(Sh) of the i^{th} particle at time t is defined as [58]:

$$Sh_i(t) = \frac{\dot{m}_i''(t)D}{\rho_{ps}D_v(Y_s - Y_\infty)} \tag{5}$$

where D_v is the diffusion coefficient of *Al* vapor in air at the particle surface. $\dot{m}_i''$ is the instantaneous average vaporization mass flux at the surface of the i^{th} particle at time t. $\dot{m}_i''$ is obtained by taking the average of local mass flux at the particle surface$(\dot{\omega}'')$ using the following equation:

$$\dot{m}_i''(t) = \frac{\oint_S \dot{\omega}'' dl}{S} \tag{6}$$

S is the perimeter (surface area in 3D) of the particle. Y_∞ in eq. (5) is the mass fraction of *Al* vapor in the free-stream flow far upstream of the particle. In the current calculations, the incoming free-stream flow does not contain any *Al* vapor; therefore, $Y_\infty = 0$. Y_s in eq. (5) is the mass-fraction of *Al* vapor in a saturated air-vapor mixture at the temperature T_l. Y_s is computed from the following relation:

$$Y_s = \frac{Mw_{Al}p_{sat}}{Mw_{air}(p_{ps} - p_{sat}) + Mw_{Al}p_{sat}} \tag{7}$$

where p_{sat} is the saturation vapor pressure of *Al* vapor at the average particle temperature T_l. p_{ps} is the post-shock pressure. Mw_{Al} and Mw_{air} are the molecular weight of *Al* and air.

The average drag force $(\overline{F_D})$, drag coefficient $(\overline{C_D})$ and Sherwood number $(\overline{Sh})$ of particles in a cluster are calculated as follows:

$$\overline{F_D} = \frac{\sum_{i=1}^{n_t} F_{D,i}(t)}{n_t} \tag{8}$$

$$\overline{C_D} = \frac{\sum_{i=1}^{n_t} C_{D,i}(t)}{n_t} \tag{9}$$

$$\overline{Sh} = \frac{\sum_{i=1}^{n_t} Sh_i(t)}{n_t} \tag{10}$$

where n_t is the number of particles immersed in the post-shock fluid at a time t.

The time-averaged Sherwood number of an isolated particle($\langle Sh \rangle$) and the particles in the cluster($\langle \overline{Sh} \rangle$) over the simulation time t_s are calculated as:

$$\langle Sh \rangle = \frac{\int_0^{t_s} Sh dt}{t_s} \tag{11}$$

$$\langle \overline{Sh} \rangle = \frac{\int_0^{t_s} \overline{Sh} dt}{t_s} \tag{12}$$

The relative difference in the time-averaged Sherwood number of the particles in a cluster and an isolated particle under the same M_s and Re_D is computed from:

$$\Delta Sh = \frac{\left| \langle Sh \rangle - \langle \overline{Sh} \rangle \right|}{\langle \overline{Sh} \rangle} \tag{13}$$

The Favre-averaged temperature($\tilde{T}$), pressure($\tilde{p}$), and velocity components along x and y-axis($\tilde{u}$ and $\tilde{v}$) of the gaseous phase within the cluster of particles are obtained from:

$$\tilde{T} = \frac{\iint \rho T dA}{\iint \rho dA} \tag{14}$$

$$\tilde{p} = \frac{\iint \rho p dA}{\iint \rho dA} \tag{15}$$

$$\tilde{u} = \frac{\iint \rho u dA}{\iint \rho dA} \tag{16}$$

$$\tilde{v} = \frac{\iint \rho v dA}{\iint \rho dA} \tag{17}$$

To quantify the deformation in the shape of the particles, an effective mean diameter,D_{eff} is defined. The D_{eff} is analogous to the definition of Sauter mean diameter for spherical particles in 3D and is defined as:

$$D_{eff} = \frac{D_A^2}{D_P} = \frac{4A_d}{S} \tag{18}$$

where D_A and D_P are the diameter of the cylinders with the same cross-sectional area and the same length of the cross-sectional perimeter of the deformed cylindrical particle, respectively. A_d is the

instantaneous cross-sectional area of the deformed cylindrical particle. D_{eff} is an "average or effective diameter" of the deformed particle. As the particle deforms, S will increase, and consequently D_{eff} will decrease. Therefore, D_{eff} quantifies the deformation of the particle, so that lower D_{eff} indicates higher deformation of the particle. $D_{eff,i}$ represents the effective mean diameter of the i^{th} particle in the cluster.

The average burn-time, t_b, of the particles in the cluster is computed from [35]:

$$t_b = \frac{\rho_{Al} D}{4\langle \overline{\dot{m}}" \rangle} \tag{19}$$

where ρ_{Al} is the density of liquid Aluminum and is taken to be 2003.0 kg/m^3. $\langle \overline{\dot{m}}" \rangle$ is the time-averaged vaporization mass-flux at the surface of the particles given by:

$$\langle \overline{\dot{m}}" \rangle = \frac{\rho_{ps} D_v (Y_s - Y_\infty) \langle \overline{Sh} \rangle}{D} \tag{20}$$

t_b is scaled as given below to compare the current calculations with the empirical correlation for burn time of Al particles obtained by Beckstead [7]:

$$t_b' = \frac{t_b X_{O_2} p_{ps}^{0.1} T_{ps}^{0.2}}{p_{atm}^{0.1}}. \tag{21}$$

where X_{O_2} is the molar concentration of oxygen, T_{ps} is the temperature in the flow behind the incident shock wave, and p_{atm} is the atmospheric pressure taken as 101325Pa.

The quantities described above are used to characterize the multiphase flow field in the calculations of shock-induced combustion of particles presented in the following section.

3. Results and Discussion

In this section, the numerical framework is first validated against benchmark results [35,59,60] and the grid independence of the current results is established. Then, the numerical framework is used to study the combustion of *Al* particle clusters under influence of shocks. The differences between the combustion of particles in a cluster and combustion of an isolated particle are investigated by comparing the flow fields and the vaporization rates. The influence of the local flow conditions characterized by the ϕ, M_s and Re_D on the flame dynamics and vaporization rates in a particle cluster is examined though the numerical calculations.

3.1 Validation

The numerical framework used in the present study has been extensively validated against several benchmark experimental [61,62] and numerical [35,60,63] results in previous publications [26,36,37,53,64,65]. Here, the multiphase flow solver is validated by comparing current results with the benchmark experimental and numerical results for shock interactions with a cylindrical water particle. The reaction kinetics solver in the current framework is verified by comparing the results for a constant volume reaction of a stoichiometric mixture of air and Al vapor with a benchmark reaction kinetics solver [66]. Results obtained for the combustion of an isolated Al particle is compared with benchmark numerical results [35] to validate the multiphase flow solver coupled with the reaction kinetics solver. Thus, each component of the numerical techniques used in performing the particle cluster simulations is separately validated in this section.

3.1.1 Comparison with the experimental results for $M_s = 1.47$ shock interaction with a cylindrical water particle of 4.8 mm in diameter

An inviscid calculation of $M_s = 1.47$ shock interaction with a cylindrical water particle of $D = 4.8mm$ is performed and the results are compared with benchmark experimental and numerical results [36,60,67]. A schematic of the initial setup of the numerical calculation is shown in Figure 1. Initially, the particle is located at $(6.25D, 6.25D)$ in the computational domain and the incoming shock is at $3.75D$. The following initial conditions are used in this calculation:

	$\boldsymbol{\rho(kg/m^3)}$	$\mathbf{p(Pa)}$	$\mathbf{u(m/s)}$
Pre-shocked air $\left(\frac{X}{D} \geq 3.75\right)$	1.0	101000	0.0
Post-shocked air $\left(\frac{X}{D} < 3.75\right)$	1.81	237792.72	247.47
Particle	1000.0	101000.0	0.0

Table 1 Initial conditions for the inviscid calculation of $M_s = 1.47$ shock interaction with a cylindrical water particle of 4.8mm in diameter.

Three different mesh resolutions corresponding to 50, 100, and 200 grid points across the particle diameter are used in this calculation. $t = 0$ is assumed at the moment of arrival of the incoming shock at the air-water interface of the particle.

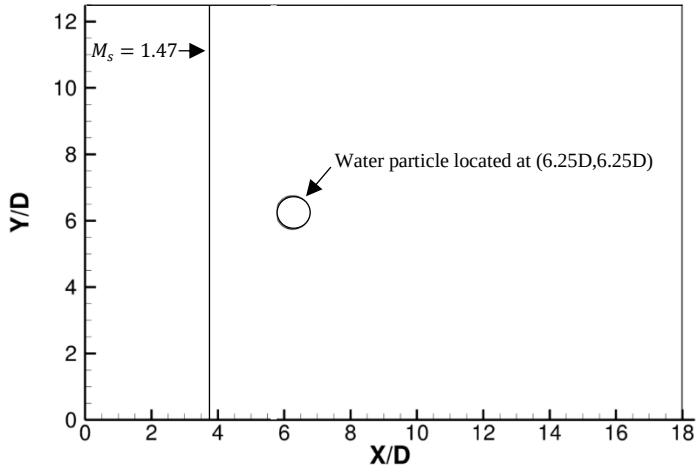

Figure 1 A schematic diagram of computational setup for the calculation of $M_s = 1.47$ shock interaction with a cylindrical water particle of 4.8 mm in diameter.

C_D of the water particle computed using the three different mesh resolutions mentioned earlier are compared with benchmark numerical results [60,67] in Figure 2(a). Discrepancies in the C_D obtained using the mesh resolutions of 50, 100, and 200 points across the particle diameter are insignificant. Therefore, the grid resolution of 100 points across the particle diameter is sufficient for this calculation.

Snapshots of the numerical Schlieren at $\frac{tu_s}{D} = 1.7$ and $\frac{tu_s}{D} = 3.38$ are compared with the experimental results [59] in Figure 2(b) and (c) respectively. A similar approach to Meng and Colonius [68] is used to match the time of snapshots in the numerical and experimental results. The results presented in Figure 2(b) and (c) show that the shape and the locations of the incident and the reflected shock predicted by the numerical calculations match closely with the experimental results. The predictions of the shape

and locations of the Mach stems and the triple points obtained from the current numerical framework also agree the experimental results. Therefore, the sharp-interface framework for compressible multiphase flows predicts the evolution of the flow-field accurately. Further comparisons of the results obtained using the current framework with benchmark experimental [62] and numerical results [60] for shock interaction with water particles can be found in [36].

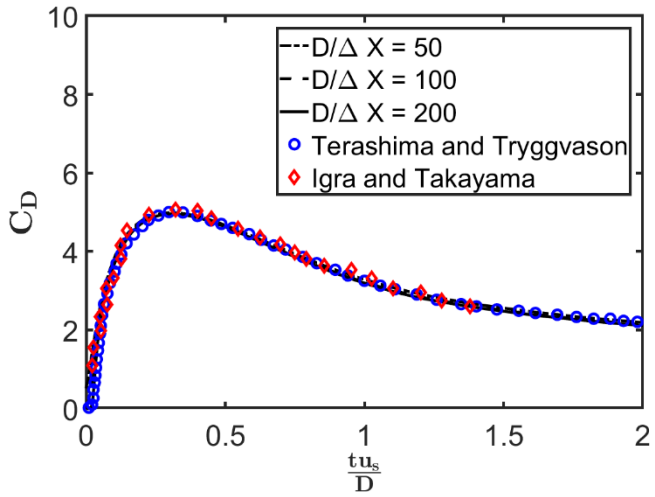

a)

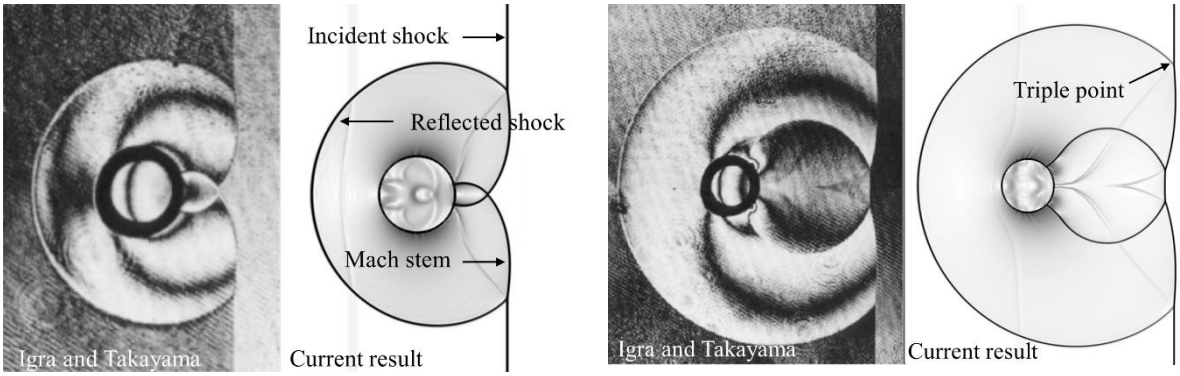

b) $\frac{tu_s}{D} = 1.7$ c) $\frac{tu_s}{D} = 3.38$

Figure 2 Comparison of current and benchmark results for $M_s = 1.47$ shock interaction with a cylindrical water particle of 4.8 mm in diameter. The drag-coefficient obtained from the current calculations using three different mesh resolutions$\left(\frac{D}{\Delta x} = 50, 100, \text{and } 200\right)$ are compared with benchmark numerical results obtained by Terashima and Tryggvason[60] and Igra and Takayama[67] in (a). The numerical Schlierens are compared with the experimental results at time $\frac{tu_s}{D} = 1.7$ and 3.38 in (b) and (c) respectively. Images in (b) and (c) are reprinted from [59] with permission from Springer.

3.1.2 Verification of the reaction mechanism solver

Constant volume reactions of the stoichiometric Al vapor-air mixture$\left(Y_{Al(g)} = 0.208, Y_{N_2} = 0.608, \text{and } Y_{O_2} = 0.184\right)$ are computed using the current reaction mechanism solver and the results are compared with the CHEMKED software [66,69]. Three different initial temperatures of the Al vapor-air mixture, viz. 2300K, 2800K, and 3000K are selected for this comparison. Figure 3(a) shows that the evolution of the temperature predicted by the current rection mechanism solver match with the CHEMKED solution [66,69] for the three initial temperatures of the mixture. Figure 3(b) shows the evolution of the mass fractions of reactants and products for reaction initiated at 2800K. The mass-fraction of all reactants and products obtained from the current reaction chemistry solver closely match with the results obtained from the CHEMKED solver [66]. Therefore, the chemical kinetics of the Al vapor-air reaction is solved accurately in the current numerical framework.

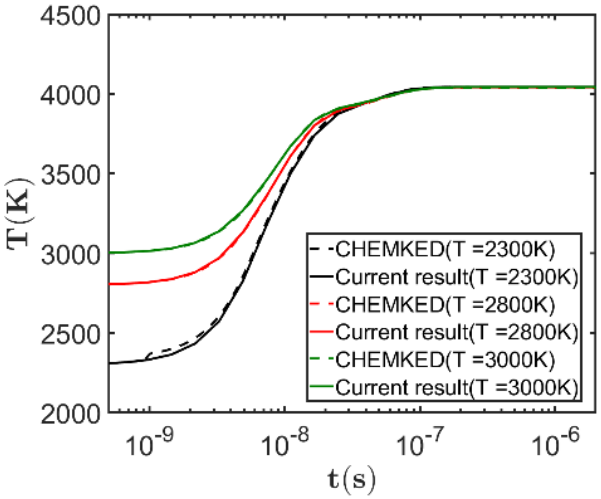

a)

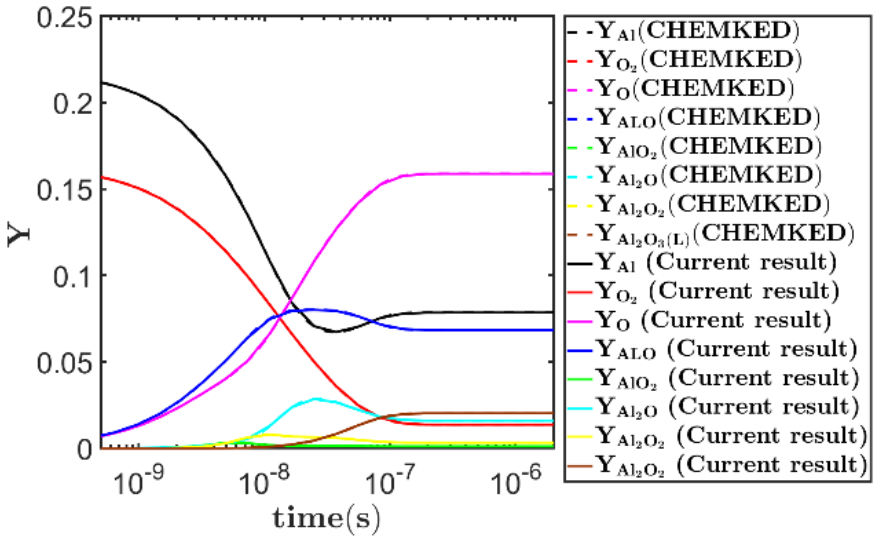

b)

Figure 3 a) The temperature rises during the constant volume reaction of the stoichiometric mixture of Al vapor and air, initiated at 2300K,2800K and 3000K.b) The evolution of the species mass-fraction during constant-volume reaction of Al vapor and air initiated at 2800K.

3.1.3 Axisymmetric calculation of Al particle combustion under the influence of a $M_s = 2$ shock

The vaporization rate of an isolated reacting Al particle under shock loading is computed and compared with an available benchmark result [35]. An axisymmetric calculation is performed for a $M_s = 2$ shock interacting with a burning Al particle, $230\mu m$ in diameter. The initial setup of the computational domain is shown in Figure 4. Neumann boundary conditions are applied at the east, west, and north sides of the computational domain. An axisymmetric boundary condition is applied at the south boundary of the domain. The calculation is initiated with a heated Al particle in quiescent flow. The particle center is initially located at $x = 0.575$mm and the following initial conditions are used:

	$\boldsymbol{\rho(kg/m^3)}$	$\mathbf{p(Pa)}$	$\mathbf{u(m/s)}$	$\mathbf{T(K)}$
Pre-shocked air $(\mathbf{x \geq 0.43mm})$	1.177	101325.0	0.0	300.0
Post-shocked air$(\mathbf{x < 0.43mm})$	3.138	455962.47	433.95	507.19
Particle	2003.0	105916.81	0.0	2750.0

Table 2 Initial conditions for the simulation of Mach 2 shock interaction with a liquid *Al* particle

The particle is resolved using 460 grid-points across its initial diameter in this study. A 9-step reaction-mechanism [35] for Al vapor-air reaction is used in this calculation to compare the current results with Houim *et al*. [35].

The temperature field around the reacting Al particle at $2\mu s$ is shown in Figure 4(b). The combustion of vaporized Al increases temperature to $\sim 3500K$ in the boundary layer and the wake of the particle. The combustion of Al vapor in the boundary layer influences vapor pressure at the particle surface and consequently vaporization rate of the particle [26,37].

The instantaneous average vaporization mass-flux$(\dot{m}")$ of the particle obtained from the current framework is compared with the benchmark result [35] in Figure 5. The $\dot{m}"$ obtained in the current study agrees with the benchmark [35] after $0.75\mu s$ of the initiation of the calculation. The discrepancy observed between the current and benchmark [35] result during the initial period of the shock-particle interaction (up to $t = 0.75\mu s$) is due to differences in the initial conditions between the two calculations. Houim et al. [35] assumed an initial layer of the heated Al vapor around the particle to suppress the initial thermally-induced acoustic wave. Adding a layer of Al vapor around the particle increases the vapor pressure around the particle immersed in the quiescent flow, thereby suppressing the initial instantaneous vaporization rate of the particle. Figure 5 therefore shows an initial lower vaporization rate of the particle in the calculation of Houim et al. [35]. Parameters defining the initial distribution of the heated Al vapor around the particle such as f_{in} and f_{out} in Eq. (53) of [70] were not mentioned in Houim et al. [35,70]. To overcome the lack of initial condition information, the presence of an initial layer of heated Al vapor is not assumed in the current study. As a result, the initial vapor pressure around the particle is lower in the current calculation than in the benchmark [35]. Due to this, the particle vaporizes at a higher rate in the current simulations during the initial stages of the shock-particle interaction. Nevertheless, once the *Al* vapor over the particle is stripped off the particle surface by the high-speed flow behind the shock, the initial Al vapor layer does not influence the vaporization rate of the particle and the quasi-steady $\dot{m}"$ computed in the current work agrees well with the benchmark result [35] after $t = 0.75\mu s$.

The vaporization mass flux $\dot{m}"$ of the particle is influenced by the convective and the diffusive transport of the Al vapor from the particle surface and the consumption of the Al vapor in the boundary layer due to chemical reactions. The agreement of the $\dot{m}"$ in the current and the benchmark result [35] indicate that the current flow solver accurately computes the vaporization of Al particle and the combustion of Al vapor in the high-speed flow.

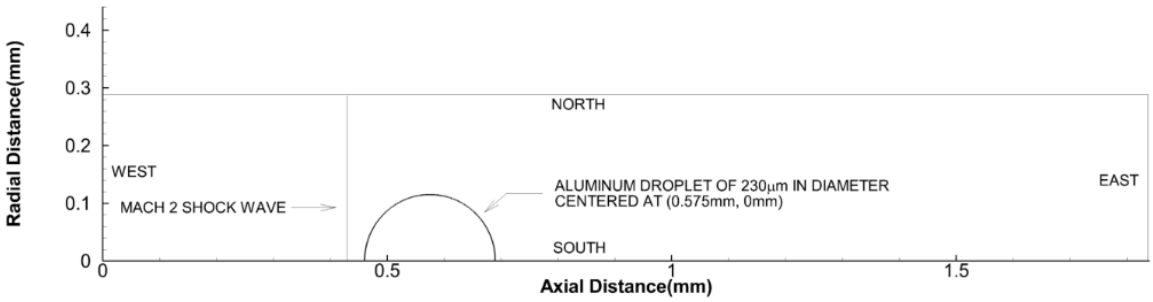

a) Initial computational setup

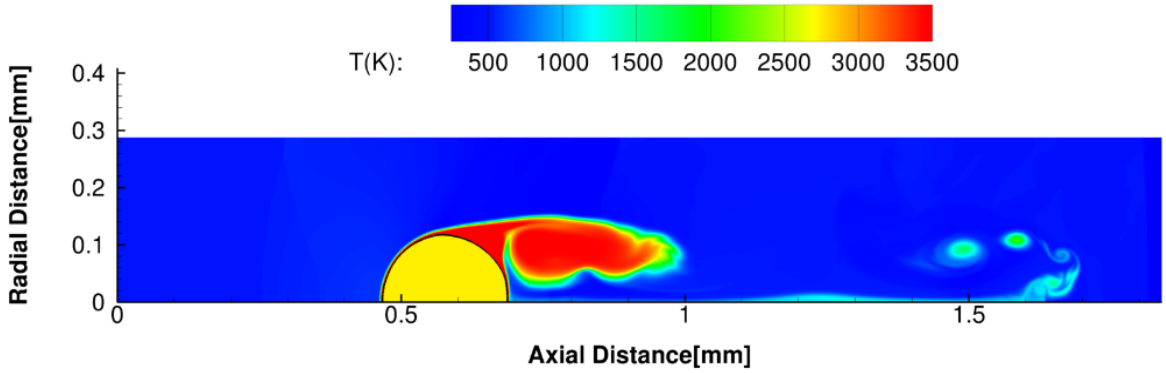

b) Temperature contour at $2\mu s$

Figure 4 (a) The initial conditions for the axisymmetric calculation of the combustion of an aluminum particle of $230\mu m$ in diameter during the interaction with an incoming Mach 2 shock.(b) Temperature contours at $2\mu s$ obtained from the axisymmetric calculation of *Al* particle combustion under the influence of Mach 2 shock.

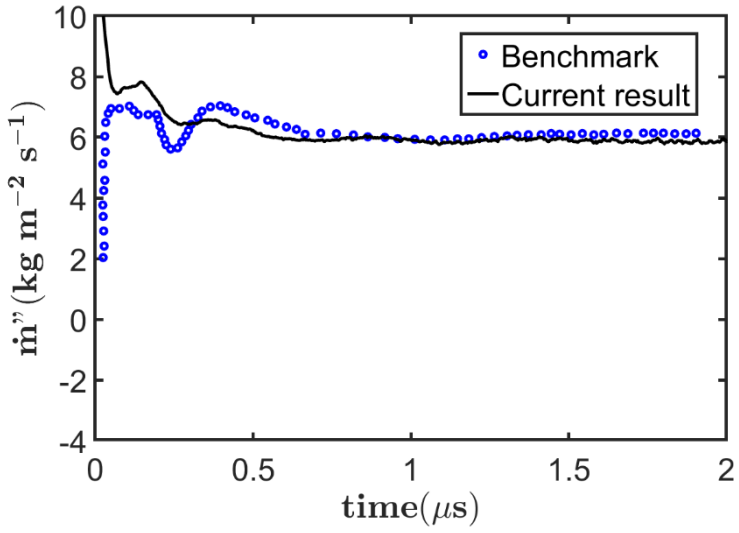

Figure 5 Comparison of the $\dot{m}''$ of the burning *Al* particle of 230μm in diameter during interaction with the Mach 2 shock obtained from the current calculation and the benchmark result [35].

3.1.4 The setup for simulation of shock interaction with clusters of reacting Al particles

As shown in the above benchmark calculations, the methods developed in this paper accurately capture the shock-interface interactions, chemical reaction progress and vaporization and burning of an *Al* particle. We now employ this framework to study the combustion of Al particle clusters in a shocked flow. The simulated conditions are relevant to the explosively dispersed Al particles carried by a blast wave [1,20]. The calculations are performed under the following assumptions/conditions:

i) After the initiation of aluminized energetic materials, the explosively dispersed Al particles are heated by the reacting post-detonation flow. As a result, the Al core of the particles melts, and Al particles are exposed to the oxidizer-rich post-detonation flow prior to their ignition. The heated Al particles develop a few nanometres thick layer of Al_2O_3 around them and do not ignite until the layer of Al_2O_3 has melted and ruptured [8,12,71]. The melting point of $Al_2O_3(2327K)$ is higher than the melting point of $Al(933K)$. Therefore, the Al core of the particles melt before they are exposed to the oxidized in the environment. The current work focuses on flame dynamics and the vaporization rate of these pure Al particles under the influence of high-speed flow entailed by shocks during the early stage after ignition. Previous experimental studies have shown that the particle surface reach $\sim 2700K$ during combustion [13,72,73]. An initial temperature of *2743K* is used for the Al particles in the current work based on the previous experimental measurements [13,72,73] and the recommendations in previous numerical studies for computing combustion of virgin Al particles [24,33,35,74,75].
ii) Prior to ignition, the initial layer of Al_2O_3 accumulate on the surface of the molten Al particle and form a small oxide cap due to the difference in surface-tensions of Al and Al_2O_3. The surface area of the oxide cap is initially significantly smaller(~5%) than the surface area of the molten Al exposed to the surrounding [49]. The oxide-cap grows later with time due to surface reactions and recondensation of the combustion products on the particle surface. However, it takes time$(\sim 10ms)$ for the oxide-cap to grow and cover a significant portion of the surface of the Al particle [49] and affect its vaporization rate. The formation and the growth of the oxide-cap on the Al particles due to the recondensation and surface reactions are ignored in the current work because the presence of oxide-cap does not affect the combustion of Al particles at the timescale of passage of the incoming shock.
iii) The objective of this work is to study the effect of particle-particle and the shock-particle interactions on the combustion of the Al particles in a cluster. Small clusters consisting of 40 randomly arranged particles are studied in the calculations. Although a cluster of randomly arranged 40 particles is found to demonstrate particle-particle interaction effects, the modest size of the particle cluster in this work limits us from studying the possibility of deflagration-to-detonation transition. The long-term evolution of larger clouds of burning particles will present a challenge to available computational resources; a route to accomplishing such calculations is possible through multi-scale modelling [26,76–79]. Computational resources also limit 3D calculations of reactive particle clusters in shocked flows, although single 3D particles have been simulated [36]. This work will be restricted to 2D simulations only.

Figure 6 shows the initial setup containing the cluster of heated pure *Al* particles of uniform initial diameter(D) randomly arranged in a cluster within a rectangular envelope in the computational domain. The length (L_c) and the width (W_c) of the cluster are calculated to maintain the desired volume fraction(ϕ) of particles within the cluster:

$$L_c = \frac{80D}{\sqrt{\phi}} \tag{22}$$

$$W_c = \frac{40D}{\sqrt{\phi}} \tag{23}$$

L_c is selected as the reference length-scale in this study. The speed of the shock-front is u_s. The time taken by the shock front to travel across the length of the cluster, i.e. $\frac{L_c}{u_s}$, is selected as the reference timescale (τ). The non-dimensional time $t^* = \frac{t}{\tau}$.

In all calculations, a Neumann boundary condition is used at the east and west boundaries, while a reflective boundary condition is used at the north and south boundaries of the computation domain. In the current calculations, the incoming shock is initially located at $\frac{x}{L_c} = 0.93$. The setup described here is used in all calculations of shock interaction with particle clusters presented in the following sections.

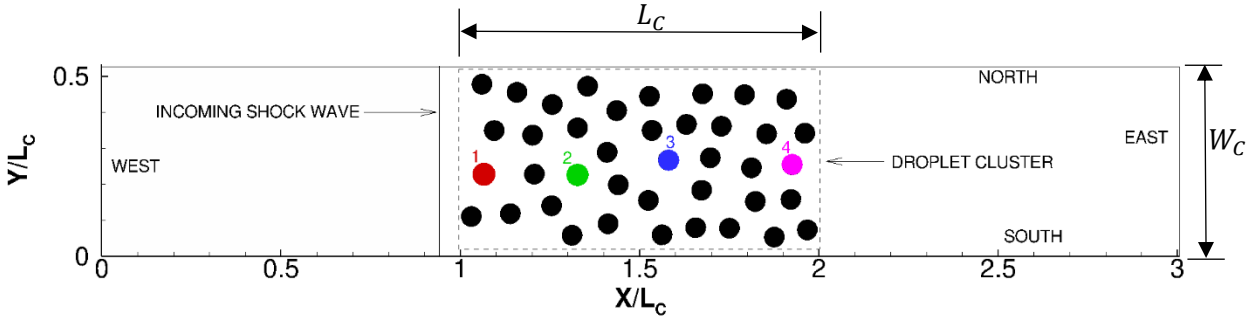

Figure 6 The initial computational setup for the numerical calculations of shock interaction with a reacting *Al* particle cluster

3.1.5 Grid independence study

As a baseline case, the combustion of a particle cluster of liquid volume fraction $\phi = 20\%$ under the influence of a $M_s = 3.5$ incoming shock at $Re_D = 1000$ is computed. The following initial conditions are used in this calculation:

	$\rho(\mathbf{kg/m^3})$	$\mathbf{p(Pa)}$	$\mathbf{u(m/s)}$	$\mathbf{T(K)}$
Pre-shocked air $\left(\frac{\mathbf{X}}{\mathbf{L_C}} \geq \mathbf{0.93}\right)$	1.204	101325.0	0.0	293.0
Post-shocked air $\left(\frac{\mathbf{X}}{\mathbf{L_C}} < \mathbf{0.93}\right)$	5.131	1431215.62	919.02	971.81
Particle	2003.0	376120.75	0.0	2743.0

Table 3 The initial conditions for the simulation of Mach 3.5 interaction with a cylindrical aluminum particle of diameter 3.84 μm.

Four different grid resolutions corresponding to 25, 50, 100, and 150 grid points across a particle diameter are used in this study. The $\overline{C_D}$ of the particles in the cluster computed using the different grid resolutions are compared in Figure 7. The relative error in the calculation of $\overline{C_D}$ for a given grid resolution is calculated as:

$$\epsilon_{\overline{C_D}} = \sqrt{\frac{\int_0^{1.5}\left(\overline{C_D} - \overline{C_{D_{GRID4}}}\right)^2 dt^*}{\int_0^{1.5}\overline{C_D}^2 dt^*}} \tag{24}$$

Grid	Resolution $\left(\frac{D}{\Delta x}\right)$	$\epsilon_{\overline{C_D}}$
GRID1	25	0.096
GRID2	50	0.057
GRID3	100	0.019
GRID4	150	-

Table 4 The relative error in the average drag obtained from the different mesh resolutions.

where $\overline{C_{D}}_{GRID4}$ is computed using the grid resolution of 150 grid points across the diameter. $\epsilon_{\overline{C_D}}$ computed from the different grid resolutions are presented in Table 4. Figure 7 shows that the $\overline{C_D}$ of the cluster converges with grid refinement. The results in Table 4 show that $\epsilon_{\overline{C_D}}$ decreases monotonically with grid refinement. 1.9% error is incurred in the $\overline{C_D}$ calculated using GRID3 relative to GRID 4, while the computational cost of using GIRD 4 is 125% more than GRID 3. To balance accuracy and computational cost, GRID3 is used in the rest of the calculation in this study.

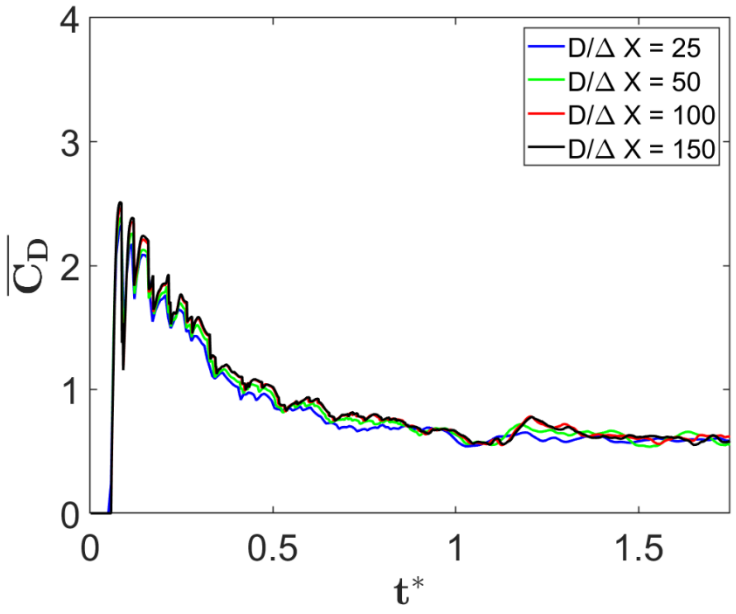

Figure 7 $\overline{C_D}$ of the particles in the cluster during interaction with a $M_s = 3.5$ shock at $Re_D = 1000$, obtained using four different grid-resolutions

3.2 Shock-induced combustion of aluminum particle clusters

Having established that the different components of the numerical approach to calculating the vaporization and combustion of an isolated Al particle are accurate, we now discuss the results for the shock-induced combustion of Al particle clusters. The effects of local flow conditions characterized by ϕ, M_s, and Re_D are studied by comparing the numerical results obtained from the following calculations:

$Case\ no.$	M_s	Re_D	ϕ
1	3.5	1000	20%
2	3.5	1000	10%
3	3.5	1000	30%
4	1.5	1000	20%
5	2.5	1000	20%
6	3.5	100	20%
7	3.5	2000	20%

Table 5 List of the numerical calculation of shock-induced combustion of Al particle clusters performed to study the effects of local flow conditions on the combustion behavior

3.2.1 Shock-induced combustion of Al particle cluster at $M_s = 3.5$ and $Re_D = 1000$

The case of $M_s = 3.5$ shock interaction with a cluster of 40 Al particles, corresponding to $\phi = 20\%$ and $Re_D = 1000$, is selected as the baseline case for this study. The combustion behaviour of the Al particles compared with an isolated particle subjected to the same M_s and Re_D. A sequence of temperature contours at four different time instances is presented in Figure 8 to elucidate the flowfield and the flame structure around individual particles in the cluster.

Evolution of flow field and combustion dynamics within the cluster

Figure 8 (a) shows the temperature contours at a time$(t^* = 0.14)$ when the incident shock has just reached the particles at the front end of the cluster. Figure 8 (b) shows that the shocklets reflected from the particles at the front end of the cluster merge to form a strong reflected shock, while the transmitted shock travels into the cluster. The $x - t^*$ plot of temperature in Figure 9 shows the propagation of the transmitted and the reflected shocks through the domain. The particle cluster resides within $1 \leq \frac{x}{L_c} \leq 2$ in Figure 9. The reflected shock traveling backward from the phase-boundary and the transmitted shock traveling further into the particle cluster are shown in Figure 9 using the markers (ii) and (iii). A system of reflected shocklets and rarefaction waves are generated due to the interaction of the transmitted shock with the randomly arranged particles. The interactions of evolving shocklets, and the rarefaction waves with the wake of the particles create an unsteady flow-field characterized by coherent structures of baroclinic vorticity [80]. Such flow unsteadiness due to shock interaction with the particle cluster distinguishes the environment experienced by a particle in the cluster from an isolated particle and results in marked differences between the flame dynamics of a reacting particle in a cluster and an isolated particle [26].

Figure 8(a) and Figure 9 show that the hot *Al* particles suspended in quiescent flow start to vaporize and react before the arrival of the incident shock. The growth of the individual diffusion flame around each particle is observed in Figure 8(a). Figure 8(b) shows that the diffusion flames around each particle grow and merge to form a deflagration front in the wake of the particle cluster. The deflagration front is indicated with the marker (iv) in Figure 9. The unreacted *Al* vapor and the oxides of Al from the particle cluster mix and react with the O_2 at the deflagration front. Figure 8 (d) shows that the temperature within the particle cluster increases after the transmitted shock has travelled across the cluster. The high-speed flow following the transmitted shock increases the convective transport of the Al vapor generated at the particle surface. The arrival of the shock also increases the concentration of O_2 in the cluster. The vortical flow in the particle wakes enhances the mixing of Al vapor and O_2 and the rate of energy release from the exothermic reaction within the cluster. The decrease in the slope at $t^* \sim 1.2$ in Figure 9 shows that the deflagration front accelerates after the arrival of the transmitted shock.

Furthermore, the onset of Richtmyer-Meshkov instabilities at the deflagration front due to the shock-flame interaction is observed in Figure 8 (d). Therefore, a high-speed and unstable deflagration front develops in the wake of the particle cluster after the passage of the transmitted shock.

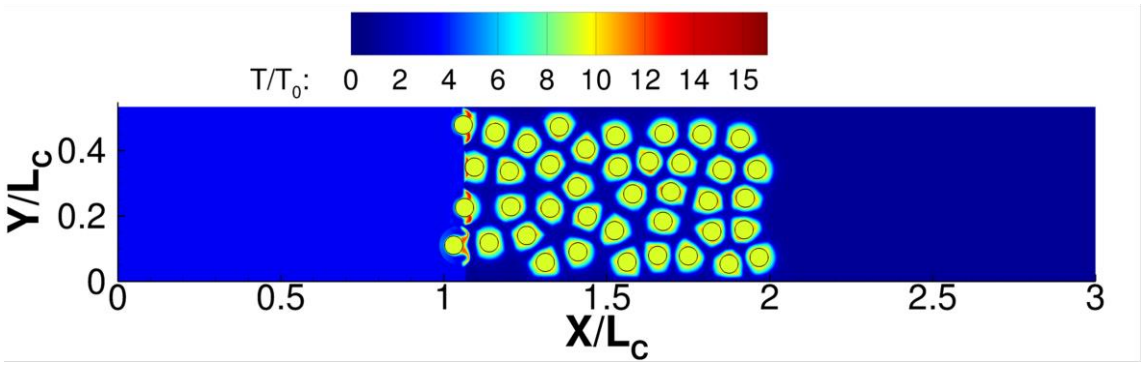

a) $t^* = 0.14$

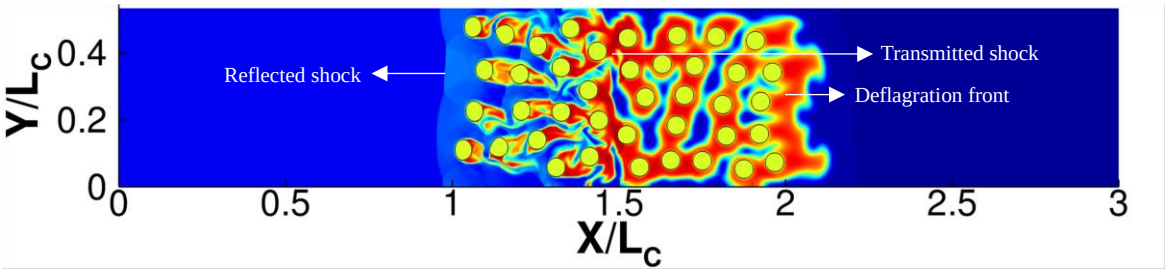

b) $t^* = 0.55$

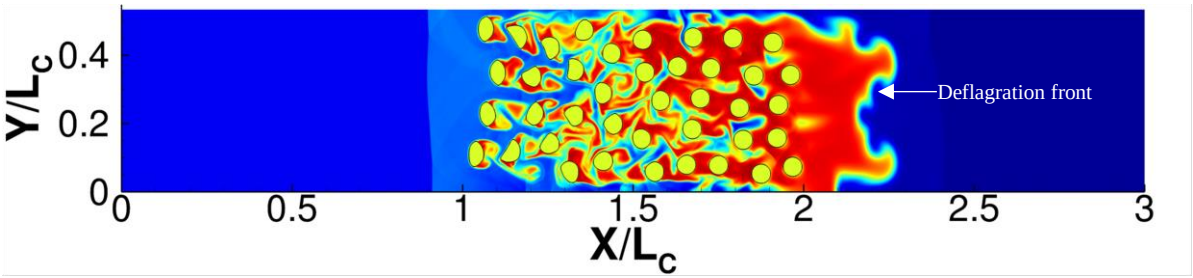

c) $t^* = 1.1$

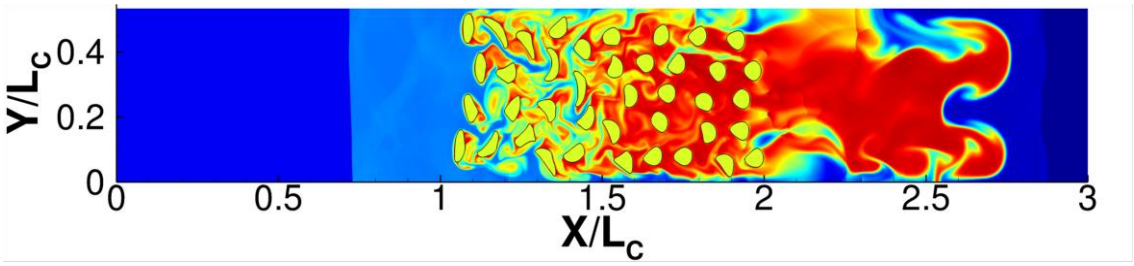

d) $t^* = 1.8$

Figure 8 A sequence of the temperature contours obtained from the reactive calculation of $M_s = 3.5$ shock interaction with an *Al* particle cluster of $\phi = 20\%$. The diameter of the particles is selected $3.844\mu m$ to ensure $Re_D = 1000$. $T_0 = 293.54K$

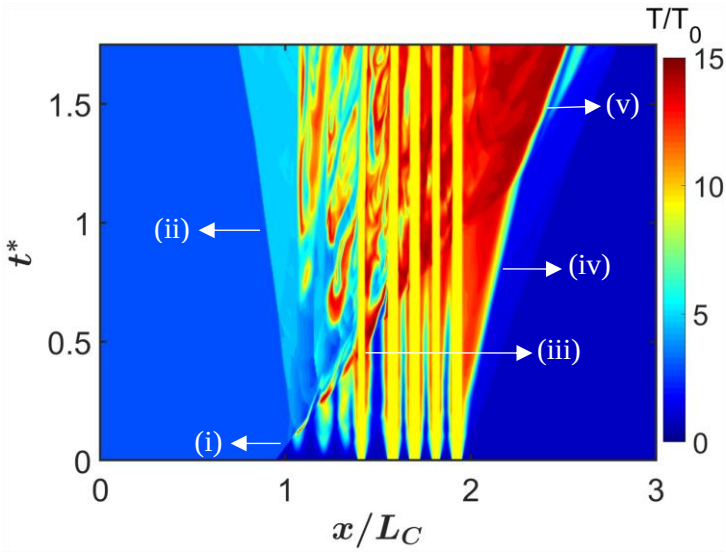

Figure 9 The $x - t^*$plots of the temperature extracted from $\frac{y}{L_c} = 0.25$ in the computational domain during the combustion of Al particle cluster of $\phi = 20\%$ under influence of an incoming $M_s = 3.5$ shock at $Re_D = 1000$. Legends: (i) Incoming $M_s = 3.5$ shock, (ii) Reflected shock, (iii) transmitted shock and (iv) diffusion flame front (v) deflagration front. $p_0 = 101325.0Pa$ and $T_0 = 293.54K$

The contour plot in Figure 8(d) and the $x - t^*$ plot of temperature along $\frac{y}{L_c} = 0.25$ in Figure 9 show that the flame structure within the particle cluster varies along the direction of shock propagation. Figure 8(d) shows that particles located at the front end of the cluster burn with unsteady wake flames [44,46]; the flamelets remain attached to and confined within the wake of the particles. Such unsteady wake flames are characteristic of kinetically-limited combustion. For particles at the front of the cluster, the flow time scale$\left(\tau_u = \frac{D}{u_{ps}} = 4.2 \times 10^{-9}s\right)$ is smaller than the reaction time scale($\tau_r \sim 10^{-7}s$). Furthermore, the shock-induced unsteadiness in the particle cluster facilitates mixing of the Al vapor and O_2 in the incoming flow. Therefore, chemical kinetics becomes the rate-limiting process during the combustion of particles located at the front end of the cluster. In contrast, Figure 8(d) shows that particles at the downstream end of the cluster burn with envelope flames [41], indicating diffusion-limited combustion. As these particles are situated in the wake of the particles upstream, they encounter a relatively low-speed incoming flow, which hinders the convective transport of the Al vapor from the surface of particles located downstream in the clusters. The Y_{Al} contours in Figure 10(a) show that the unreacted Al vapor accumulates at the downstream end and in the wake of the particle cluster. Figure 10(b) shows a gradual decrease in the concentration of O_2 along the flow direction in the particle cluster. Under the combined influence of the above factors, the particles in the downstream part of the cluster burn in an oxygen-lean environment. The lack of mixing of the Al vapor and O_2 at the downstream end of the particle cluster further limits the reaction. Therefore, the mode of combustion across a particle cluster changes from kinetically-limited to diffusion-limited, even for the rather small cluster simulated in the current work.

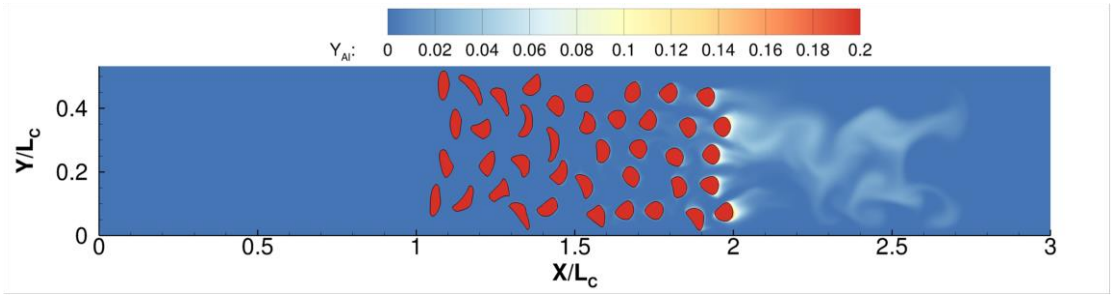

a)

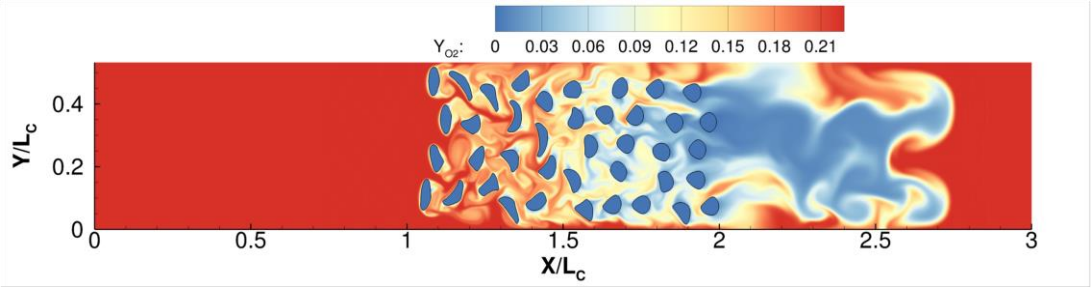

b)

Figure 10 The contours of (a) Y_{Al} and (b) Y_{O_2} at $t^* = 1.8$ obtained from the reactive calculation of $M_s = 3.5$ shock interaction with a cluster of Al particle($\phi = 20\%, Re_D = 1000$).

$D_{eff}, C_D,$ and Sh of particles in a cluster compared with an isolated particle

The above results show that the following two key physical mechanisms are found to significantly influence the combustion of particles in a cluster: 1) wake-particle interaction, and 2) the shock-induced unsteadiness in the flow-field. As shown above, the shock-induced unsteadiness in a particle cluster encourages mixing of Al vapor with O_2 in the incoming flow. However, interaction with the wake of upstream particles limits the transport and mixing of the Al vapor produced by particles located downstream in the cluster. Both these mechanisms are absent during the combustion of an isolated particle. The role of these mechanisms in influencing the drag and vaporization rate of the reacting particles in a cluster are examined by comparing these quantities with isolated particles in the following subsections.

The presence of a particle in a cluster will influence the mass, momentum, and energy exchange with the surrounding gas, leading to differences in deformation, vaporization, and combustion rates of the individual particles in the cluster. Quantitative measures of these effects, viz. $D_{eff}, C_D,$ and Sh for four selected particles (identified in Figure 6) are plotted in Figure 11(a), (b), and (c) respectively. The $D_{eff}, C_D,$ and Sh of these four particles are also compared with the cluster averages and with the corresponding measures for an isolated particle.

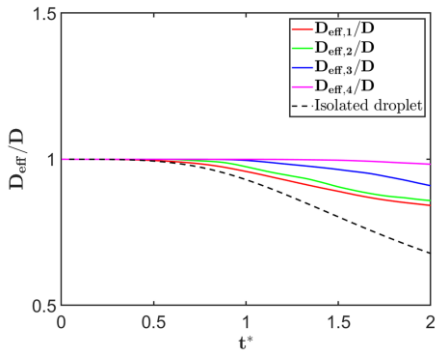

a)

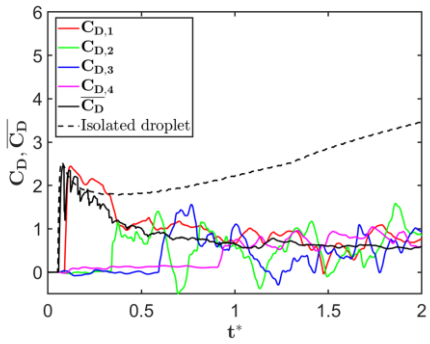

b)

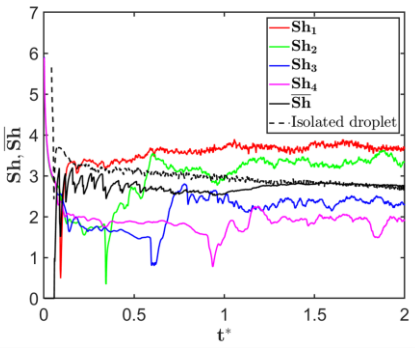

c)

Figure 11 a) C_D, b) D_{eff}, and c)Sh of four selected particles in the cluster of 20% volume fraction during the interaction with the $M_s = 3.5$ shock. The C_D,Sh and D_{eff} of the individual particles in the cluster are compared with the $\overline{C_D}$ and $\overline{Sh}$ of the whole cluster and an isolated particle.

Figure 11(a) compares the time evolution of particle size D_{eff} of the four particles, showing that the particles at the front of the cluster attain lower D_{eff} , i.e. they deform more than the particles in the trailing end of the cluster. Figure 11(b) shows that the peak C_D of the particle at the front end of the cluster (i.e. particle 1) is higher than the other three downstream particles. The C_D of an isolated particle is compared with the four particles in the cluster in Figure 11(b); the peak drag of an isolated particle is comparable with the particle at the leading edge. The C_D of the isolated particle decreases momentarily after the shock has traveled past it. However, Figure 11(b) shows that at later times the C_D

of the isolated particle increases, in contrast to the decrease of C_D of the particles in the cluster. The greater deformation of the isolated particle contributes to the recorded high C_D at later times. The averaged drag coefficient $\overline{C_D}$ is computed using Eq. (9) and shown in Figure 11(b). The $\overline{C_D}$ is initially high as the incoming shock impinges on the particles at the leading edge of the cluster. However, $\overline{C_D}$ decreases as the transmitted wave travels through the cluster [65].

An isolated particle is exposed to a higher pressure gradient and therefore deforms more rapidly than particles in the cluster. The pressure drops suddenly in the wake of an isolated particle during the shock-interaction due to the rapid expansion of the supersonic flow. However, the pressure drops gradually across a particle cluster because of the resistance to the flow provided by the other particles in the vicinity [81]. This leads to lower pressure gradients across particles in the downstream part of the cluster resulting in lower vaporization rates, drag, and deformation than an isolated particle.

The non-dimensional mass flux Sh from the four particles marked in Figure 6 and an isolated particle is shown in Figure 11(c). In comparison with the isolated particle, the particles closer to the front end of the cluster vaporize at a higher rate while the particles near the downstream end of the cluster vaporize at a lower rate. This is because the shock-induced unsteadiness in the flow field enhances the mixing of the *Al* vapor produced at the particle surface with the incoming air. This enhanced mixing increases the rate of transport of *Al* vapor from the particle surface and the vapor pressure around the particles decreases. The lower vapor pressure leads to a higher vaporization rate and Sh of the particles at the front end of the cluster compared to an isolated particle. However, the particles at the trailing end of the cluster vaporize at a lower rate than the isolated particle as they interact with the low-speed wake of the upstream particles. The relatively low flow velocity at the downstream end of the particle cluster suppresses the convective transport of Al vapor from the particle surface. Furthermore, as the unreacted Al is convected downstream, the concentration and vapor pressure of unreacted Al vapor around the particles in the downstream end of the cluster increase. Therefore, the vaporization rate of particles in a cluster is dictated by two competing physical mechanisms: enhancement in mixing due to the shock-induced unsteadiness and suppression of mixing due to the wake-particle interaction. The overall result is a low vaporization rate of particles located at the downstream end of the cluster.

The cluster-averaged Sherwood number $\overline{Sh}$ is shown in Figure 11(c) for the present case of $M_s = 3.5, Re_D = 1000$ and $\phi = 20\%$. The $\overline{Sh}$ of the cluster is comparable with the vaporization rate of an isolated particle. The time-averaged Sherwood number of the particles in the cluster $\langle\overline{Sh}\rangle$ is 2.7, while the time-averaged Sherwood number of the isolated particles $\langle Sh\rangle$ is 2.97. The relative difference in the vaporization rates of the particles in a cluster and an isolated particle ΔSh is 0.092. Therefore, the average vaporization rate of particles in a cluster is only 9.2% less than the vaporization rate of an isolated particle for the present M_s and Re_D. However, the value of ΔSh changes with $\phi, M_s,$ and Re_D. The mechanistic details of how $\phi, M_s,$ and Re_D influence the combustion and the vaporization rate of particles in a cluster are examined next.

3.2.2 Effects of volume fraction ϕ on the combustion of particles in a cluster

The effects of ϕ are studied by simulating the combustion of Al particle clusters at $\phi = 10\%, 20\%,$ and 30% under the influence of a $M_s = 3.5$ shock and $Re_D = 1000$. The simulations for all volume fractions are set up as described in section 3.1.4.

Figure 12 compares the Favre-averaged temperature $(\tilde{T})$, pressure $(\tilde{p})$, and axial velocity$(\tilde{u})$ for the three different values of ϕ. Figure 12 (a) and (b) show that the pressure and temperature in the cluster increase with the particle loading ϕ; the amount of Al vapor released in the gas phase also increases with ϕ, leading to an increase in the chemical energy release. Figure 12 (c) shows that during the shock interaction, $\tilde{u}$ in the cluster decreases with the increase in ϕ. Therefore, the momentum transferred from the gas phase to the liquid phase increases with ϕ, suppressing the flow unsteadiness in the gas phase. This decrease in momentum in the gas phase with an increase in ϕ influences the rate of transport and mixing of species and ultimately the combustion in the particle cluster.

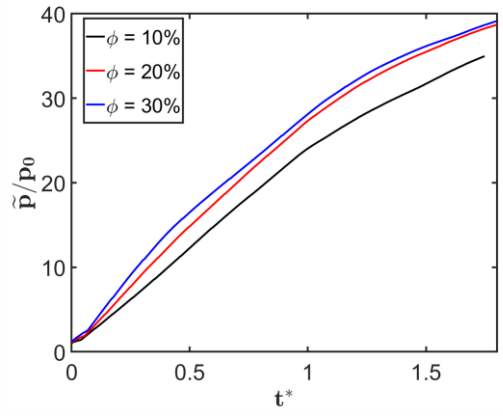

a)

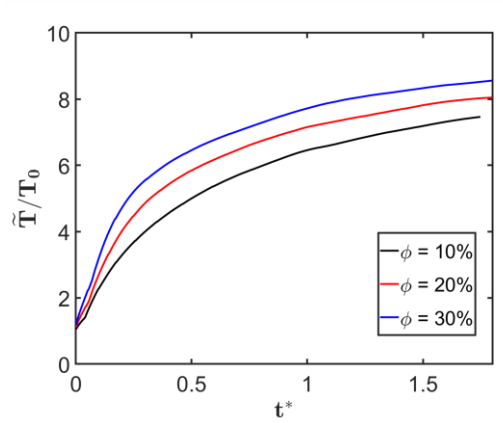

b)

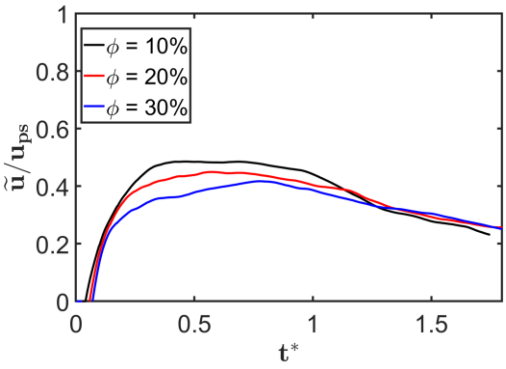

c)

Figure 12 The comparison of the Favre averaged (a)pressure$(\tilde{p}/p_0)$, (b)temperature$\left(\tilde{T}/T_0\right)$, and (c)axial velocity$(\tilde{u}/u_{us})$ of the gas-phase within the particle clusters with $\phi = 10\%, 20\%$ and 30% during the interaction with $M_s = 3.5$ shock. The initial diameter of the particles is $3.844\mu m$ and the corresponding Re_D is 1000. $p_0 = 101325.0Pa$ and $T_0 = 293.54K$

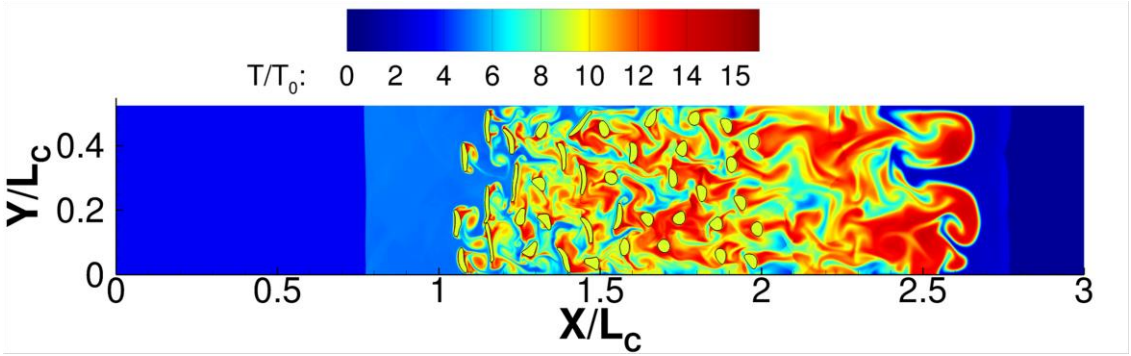

$a)\ \phi = 10\%$

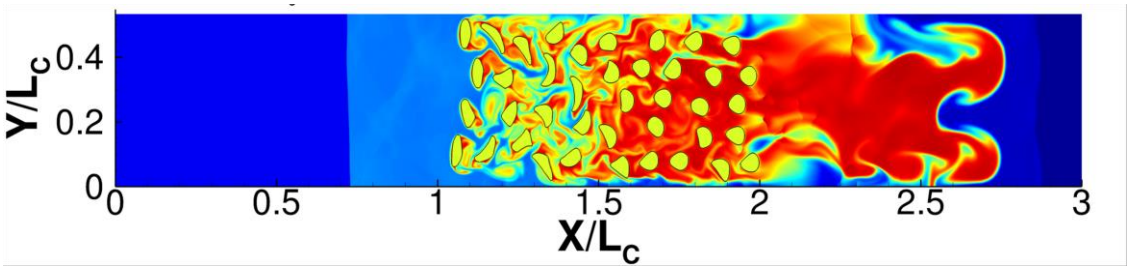

$b)\ \phi = 20\%$

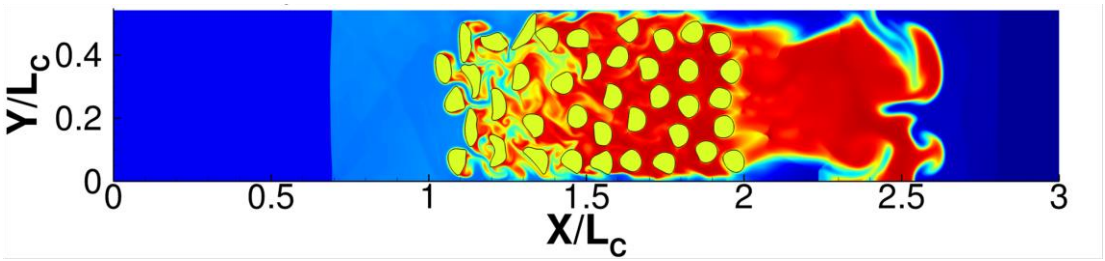

$c)\ \phi = 30\%$

Figure 13 The temperature contours during the $M_s = 3.5$ shock interaction with cluster of particles of volume-fractions a) $\phi = 10\%$, b) $\phi = 20\%$, and c) $\phi = 30\%$ at $t^* = 1.73$. The initial diameters of the particles are $3.844\mu m$. $T_0 = 293.54\ K$

Figure 13 compares temperature contours within the Al particle cluster for $\phi = 10\%, 20\%,$ and 30% at $t^* = 1.73$. In Figure 13 (a), for $\phi = 10\%$, the flamelets are found to be sporadically distributed within and in the wake of the particle cluster indicating kinetically-limited combustion; most particles in the relatively dilute cluster burn with an unsteady wake flame. At higher loadings, $\phi = 20\%$ and 30%, the particles near the downstream end of the cluster burn with an envelope flame exhibiting the characteristics of diffusion-limited combustion.

The $\overline{Sh}$ of the particles in the clusters for $\phi = 10\%, 20\%,$ and 30% are compared in Figure 14(a). Figure 14(a) shows that the $\overline{Sh}$ decreases with increase in ϕ. The average vaporization rate of the particles in the cluster for $\phi = 10\%, 20\%,$ and 30% are respectively 5.4%, 8.5%, and 15.0% less than that of an isolated particle at $M_s = 3.5$ and $Re_D = 1000$ flow. This is due to the increase in unreacted Al vapor and the subsequent increase in Al vapor pressure at the surface of the particles in a cluster at higher ϕ.

3.2.3 *Effects of M_s on the combustion of particles in a cluster*

The effect of shock strength on combustion of a particle cluster is investigated for shocks with $M_s = 1.5, 2.5,$ and 3.5. Clusters of randomly arranged particles at $\phi = 20\%$ and $Re_D = 1000$ are placed in the computational setup described in section 3.1.4.

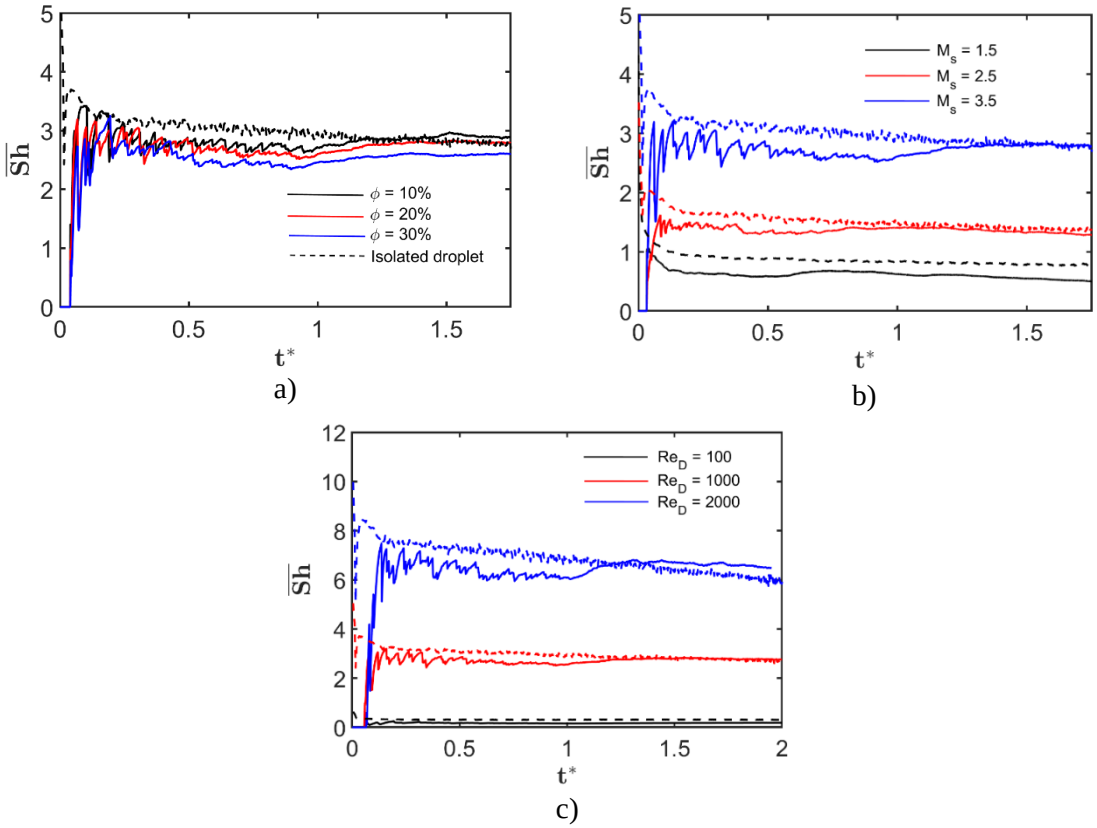

Figure 14 $\overline{Sh}$ of the particles in the clusters are compared with the Sh of isolated particles in (a), (b), and (c) for different flow conditions characterized by M_s, Re_D , and ϕ.(a) shows the comparison of $\overline{Sh}$ for $\phi = 10\%$, 20%, and 30% with an isolated particle at $M_s = 3.5$ and $Re_D = 1000$. (b) shows how $\overline{Sh}$ in a cluster of particles vary with M_s. The $\overline{Sh}$ in a particle cluster for $M_s = 1.5, 2.5,$ and 3.5 are compared with an isolated particle sujected to the respective M_s. $Re_D = 1000$ and $\phi = 20\%$ in these calculations. (c) shows the effect of Re_D on the $\overline{Sh}$ of the particles. $Re_D = 100, 1000,$ and 2000 are selected for this comparison. $M_s = 3.5$ and $\phi = 20\%$ in these calualtions. In (b) and (c), solid lines show the $\overline{Sh}$ of the particle cluster and the dashed lines of the same color show the Sh of an isolated particle for the respective $M_s$and Re_D

Insights into the combustion process in the Al particle cluster can be obtained from the temperature contours at $t^* = 1.73$ plotted in Figure 15 for the three shock strengths. Figure 15 (a) shows that the entire particle cluster exhibits the flame characteristics of diffusion-limited combustion at $M_s = 1.5$. For $M_s = 1.5$, the flow timescale$\left(\tau_u = \frac{D}{u_{ps}} = 1.4 \times 10^{-7} s\right)$ and the mass-diffusion timescales$\left(\tau_D = \frac{D^2}{D_{Al,mix}} = 3.32 \times 10^{-6} s\right)$ are larger than the reaction timescale ($\tau_r \sim 10^{-7} s$). Therefore, combustion of the particles in the cluster is limited by the transport and mixing processes at $M_s = 1.5$.

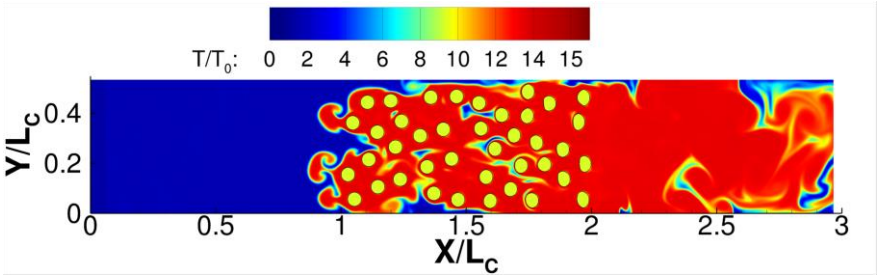

a) $M_s = 1.5$

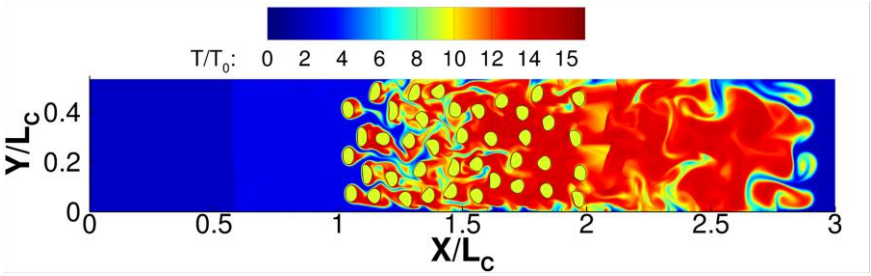

b) $M_s = 2.5$

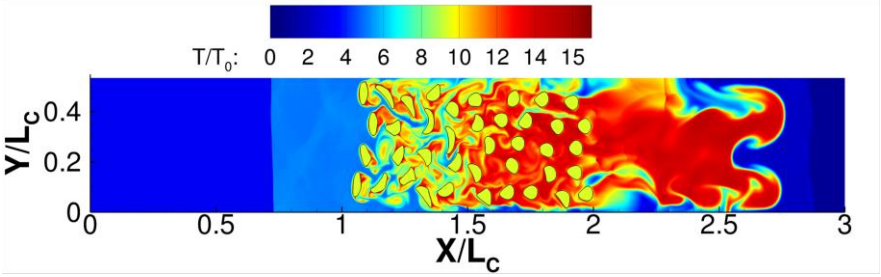

c) $M_s = 3.5$

Figure 15 The temperature contours during the (a) $M_s = 1.5$, (b) $M_s = 2.5$, and (c) $M_s = 3.5$ shock interaction with cluster of particles of volume-fraction $\phi = 20\%$ at $t^* = 1.73$. $Re_D = 1000$ for all three cases. $T_0 = 293.54K$

Figure 15 (b) and (c) show that the distributed unsteady flamelets appear at the front end of the particle cluster when M_s is increased to 2.5 and 3.5. Figure 15 shows that the region of envelope flame characterizing diffusion-limited combustion shifts downstream in the cluster when M_s is increased.

The $\overline{Sh}$ for particles in the cluster during interaction for $M_s = 1.5, 2.5,$ and 3.5 are compared in Figure 14(b). The observed increase in $\overline{Sh}$ of particles at higher M_s has been noted in previous works [26,37]. Figure 14(b) shows that the $\overline{Sh}$ of particles in the cluster is less than the value for isolated particles for a given M_s. Specifically, the average vaporization rate of the particles in a cluster with $\phi = 20\%$ subjected to $M_s = 1.5, 2.5,$ and 3.5 shocks are respectively 28.9%, 9.9%, and 8.5% less than that of an isolated particle.

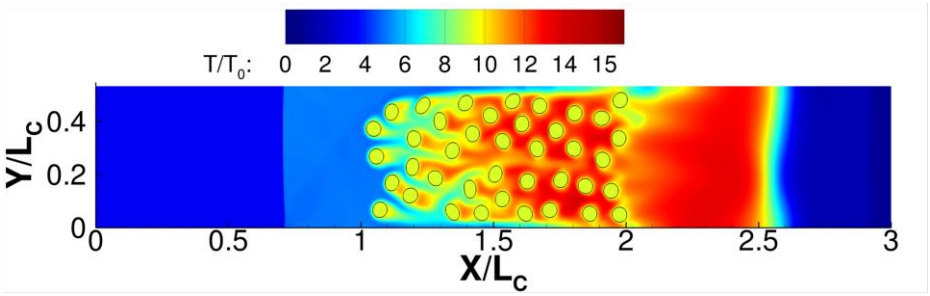

$a)\ Re_D = 100$

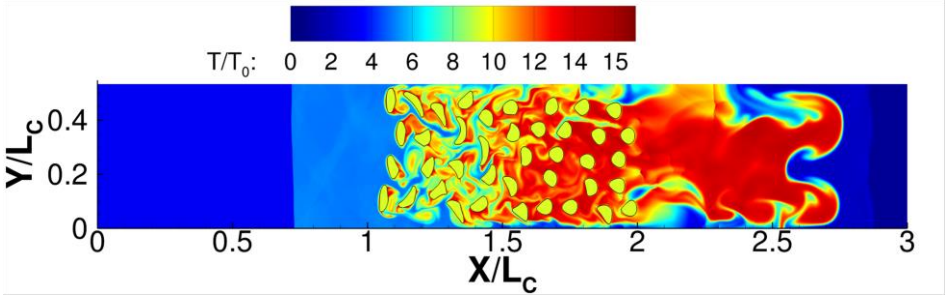

$b)\ Re_D = 1000$

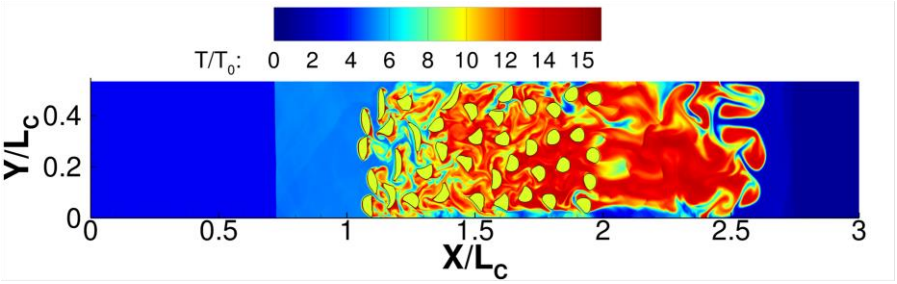

$c)\ Re_D = 2000$

Figure 16 The temperature contours during $M_s = 3.5$ shock interaction with particles clusters of $\phi = 20\%$ and a) $Re_D = 100$ b) $Re_D = 1000$ and c) $Re_D = 2000$ at $t^* = 1.73$. $T_0 = 293.54K$

3.2.4 Effects of particle size (Re_D) on the combustion of the particles in a cluster

Numerical calculations of $M_s = 3.5$ shock interaction with Al particle clusters at $Re_D = 100, 1000, \text{and } 2000$ ($D = 0.3844\mu m, 3.844\mu m, \text{and } 7.688\mu m$ respectively) are performed in the computational set-up described in section 3.1.4. The particle clusters are designed to achieve $\phi = 20\%$. The temperature contours for $Re_D = 100, 1000, \text{and } 2000$ at are compared in Figure 16, which is plotted in non-dimensional spatial coordinates and time $t^* = 1.73$. The temperature contours in Figure 16 show that the unsteadiness in the flow field decreases with Re_D. Since unsteadiness in the flow field is conducive to the mixing of Al vapor generated at the particle surface with the O_2 in the incoming flow, mixing in the cluster is hindered when Re_D decreases. However, mixing through the diffusive transport increases at the low Re_D. When Re_D increases to 1000, Rayleigh-Taylor(R-T) instabilities at the deflagration front are observed in the temperature contours in Figure 16 (b). At $Re_D = 2000$, flame structures with smaller length-scales emerge at the deflagration front.

The effect of Re_D on the vaporization rate of the particles is depicted in Figure 14(c) by comparing $\overline{Sh}$ of the particles in the cluster at the three values of $Re_D = 100, 1000, \text{and } 2000$. Figure 14(c) shows that the $\overline{Sh}$ of the particle cluster increases with Re_D. This is because the rate of diffusive transport of

the *Al* vapor from the particle surface decreases with an increase in Re_D [37]. Furthermore, Figure 14(c) shows that the vaporization rate of the reacting particles in the cluster is lower than the vaporization rate of isolated particles subjected to the same Re_D. The average vaporization rate of the particles in a cluster with $\phi = 20\%$ subjected to $M_s = 3.5$ shock at $Re_D = 100, 1000, \text{and } 2000$ is respectively 44.0%, 8.5%, and 6.6% less than that of an isolated particle subject to the same M_s and Re_D.

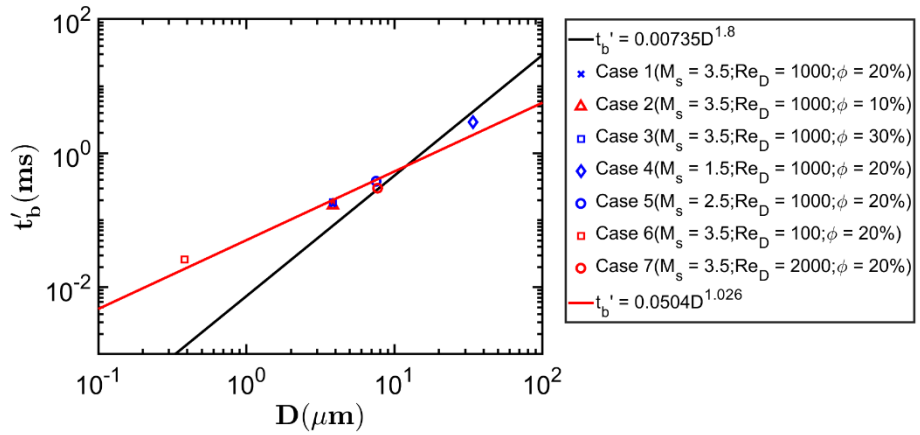

Figure 17 The scaled burn-time(t_b') of the Al particles in the cluster obtained from the current calculations is plotted against the corresponding initial particle diameter(D). Current results are compared with the empirical correlation between $t_b{}'$ and D obtained by Beckstead[7] from experimental data. The black line shows the empirical correlations obtained from experiments in [7]. The symbols show the burn-time of Al particle clusters in shocked flows obtained from the current calculations. The red line is a linear least square fit to the $\log_{10} t_b{}'$ vs $\log_{10} D$.

3.3 Burn-time of the Al particles in shocked flows and relationship to flame dynamics

The scaled average burn-time (t_b') of the Al particles in the current calculations is estimated using Eq. (19) - (21) and plotted against the particle diameter D in Figure 17. t_b' obtained from current calculations are compared with an empirical correlation between t_b' and D obtained by Beckstead [7] from experimental data:

$$t_b' = 0.00735D^{1.8} \tag{25}$$

A linear least-squares fit to $\log_{10} t_b'$ vs $\log_{10} D$ in the current calculations gives:

$$t_b' = 0.0504D^{1.026} \tag{26}$$

The correlations in Eq. (25) and (26) are shown by the black and red lines in Figure 17, respectively. Figure 17 shows that the burn-time of the Al particles computed from the current simulations are in the same range of the predictions obtained from the benchmark correlation given in Eq. (25) [7]. However, the exponent of D in the t_b' vs D relation(Eq. (26)) obtained from the current calculations is smaller than the exponent obtained by Beckestead [7]. The exponent of D obtained by Beckstead [7] is closer to 2. This is because, the empirial correlation was obtained from the experimental measurements of the burn-time of larger Al particles($D = 10 - 1000\ \mu m$) in quiescent or low-speed flow conditions [7]. Under such conditions, the Al particles are more likely to undergo diffusion limited combustion. As a result, the exponent of D in the t_b'vs D correlation describing these experimental results(Eq. (25)) is closer to the theoretical $t_b \propto D^2$ law for diffusion-limited combustion. On contrary, the exponent of D in the correlation between t_b' and D obtained in the current calculation(Eq. (26)) is 1.026; the almost linear dependence of t_b' on D in the current calculation indicate kinetically limited combustion of the Al particles in shocked flows. The dominant effect of convection in shocked flows pushes the combustion dynamics of Al particle clusters towards kinetically limited combustion regime, where $t_b \propto D$ [1]. The

temperature contours in Figures 13, 15, and 16 in the previous subsection show that Al particle located upstream in the cluster exhibit unsteady wake-flames indicating kinetically- limited combustion under the influence of high-speed flow behind the shock, while particles located downstream in the cluster most likely to burn with a diffusion flame. As a result, the average burn-time of the Al particles in the cluster under shocked conditions are not well represented by the burn-time correlations derived from experimental studies of Al particle combustion in the diffusion limited regime.

4. Conclusions

The combustion of aluminum particle clusters in shocked flows is studied through interface-resolved numerical calculations. The current work examines the flame dynamics and the burning rate of aluminum particle clusters under various shock Mach numbers (M_s), Reynolds numbers (Re_D), and particle volume fractions (ϕ).

The flame dynamics during the combustion of particles in a cluster is found to be remarkably different from that of an isolated particle. At $M_s = 3.5$ and $Re_D = 1000$, an isolated particle burns with a quasi-steady wake flame characterizing kinetically-limited combustion. In contrast, the flame-structure around a particle within a cluster varies along the direction of the flow. Particles at the front end of the cluster undergo kinetically-limited combustion with the formation of a wake flame, while, particles located downstream in the cluster burn with an envelope-flame indicating combustion limited by transport and mixing. The transition in the flame-structure from the front to the back end of the cluster is attributed to the following competing effects which are absent in the case of an isolated particle:

i) Baroclinic vorticity-induced unsteadiness in the flow field produced during the passage of the incoming shock through the particle cluster.
ii) The interaction of the particles downstream in the cluster with the wake of the particles located upstream.

The baroclinic vorticity-induced unsteadiness in the particle cluster enhances micro-mixing. On the other hand, the interaction with the low-speed oxygen-deficient wake of the particles upstream limits the convective transport, mixing and combustion of the aluminum vapor produced at the surface of particles. Since the fuel-air ratio in a cluster increases at higher volume fractions, the number of particles enveloped in a diffusion-limited flame within the cluster increases with increasing volume fraction. Collectively, the results show that the vaporization rate of a particle in a cluster is significantly lower than the vaporization rate of an isolated particle under the same flow conditions. Therefore, models for vaporization rate of aluminum (fuel) particles in a high-speed flow must take into account the effects of volume fraction.

Aside from particle-particle interactions, shock-particle interactions also exert significant influences on vaporization and combustion in a cluster. The average Sherwood number$(\overline{Sh})$ of the reacting particles in the cluster show a significant increase with increasing M_s. The change in Re_D (particle size) also significantly influences the flame dynamics and the burning rate of the particles in the cluster. At lower Reynolds number $(e.g. Re_D = 100)$ viscous dissipation suppresses unsteadiness in the flow field and at the deflagration front. At higher Reynolds numbers convective transport and unsteady vortical mixing becomes the dominant mechanism for mixing in the cluster. Therefore, the $\overline{Sh}$ of the particles within the cluster increases with the increase in Re_D.

This work is the first investigation of the detailed thermomechanics of particle clusters in a high-speed gas flow and provides new insights into the vaporization and flame dynamics at the length scale of individual aluminum particles under conditions not easily accessed by physical experiments. However, the results are limited by the size of the particle cluster used in this study, which precludes the observation of the deflagration to detonation transition during the combustions of micron size particles. Studies on the effects of cluster size on flame and wave propagation through the cluster will be pursued in future work. Furthermore, the current work has been limited to 2D calculations only. The interaction of the shocks and the flamelets in the turbulent flow field and their effects on the burning rate of the particles in the cluster cannot be studied using the present 2D calculations. 3D calculations of particle cluster combustion are currently being pursued and will be reported in the future.

5. Acknowledgments

The authors gratefully acknowledge the financial support from the Air Force Research Laboratory Munitions Directorate (AFRL/RWML), Eglin AFB, under contract number FA8651-16-1-0005 , Pratik Das acknowledges the generous financial support received through S. K. Nanda Engineering scholarship (2017 and 2018) and Sharda Devi Planjery Memorial Award (2019).

6. Data availability

The data that support the findings of this study are available from the corresponding author upon reasonable request.

7. References

[1] V. Tanguay, S. Goroshin, A. J. Higgins, and F. Zhang, Aluminum Particle Combustion in High-Speed Detonation Products, Combust. Sci. Technol. **181**, 670 (2009).

[2] M. A. Cook, A. S. Filler, R. T. Keyes, W. S. Partridge, and W. Ursenbach, Aluminized Explosives, J. Phys. Chem. **61**, 189 (1957).

[3] D. S. Sundaram, P. Puri, and V. Yang, A General Theory of Ignition and Combustion of Nano- and Micron-Sized Aluminum Particles, Combust. Flame **169**, 94 (2016).

[4] F. Zhang, K. Gerrard, and R. C. Ripley, Reaction Mechanism of Aluminum-Particle-Air Detonation, J. Propuls. Power**25**, 845 (2009).

[5] V. Tanguay, Combustion of Reactive Metal Particles in High-Speed Flow of Detonation Products, Ph.D. thesis, McGill University (Canada), 2008.

[6] A. Davis, Solid Propellants: The Combustion of Particles of Metal Ingredients, Combust. Flame **7**, 359 (1963).

[7] M. W. Beckstead, Correlating Aluminum Burning Times, Combust. Explos. Shock Waves **41**, 533 (2005).

[8] T. A. Brzustowski and I. Glassman, Spectroscopic Investigation of Metal Combustion, in *Progress in Astronautics and Rocketry*, edited by H. G. Wolfhard, I. Glassman, and L. Green, Vol. 15 (Elsevier, 1964), pp. 41–73.

[9] A. S. Boreisho, A. V. Ivashchenko, and G. G. Shelukhin, Problem of Determining the Sizes of Burning Metal Particles, Combust. Explos. Shock Waves **11**, 561 (1975).

[10] E. L. Dreizin and M. A. Trunov, Surface Phenomena in Aluminum Combustion, Combust. Flame **101**, 378 (1995).

[11] T. Bazyn, H. Krier, and N. Glumac, Evidence for the Transition from the Diffusion-Limit in Aluminum Particle Combustion, Proc. Combust. Inst. **31**, 2021 (2007).

[12] V. Sarou-Kanian, J. C. Rifflet, F. Millot, and I. Gökalp, Aluminum Combustion in Wet and Dry CO2: Consequences for Surface Reactions, Combust. Flame **145**, 220 (2006).

[13] J. C. Melcher, H. Krier, and R. L. Burton, Burning Aluminum Particles Inside a Laboratory-Scale Solid Rocket Motor, J. Propuls. Power**18**, 631 (2002).

[14] C. Miller, S. Kim, Y. Horie, and M. Zhou, Ignition Thresholds of Aluminized HMX-Based Polymer-Bonded Explosives, AIP Advances **9**, 045103 (2019).

[15] H. M. Cassel and I. Liebman, The Cooperative Mechanism in the Ignition of Dust Dispersions, Combust. Flame **3**, 467 (1959).

[16] K. Balakrishnan, A. L. Kuhl, J. B. Bell, and V. E. Beckner, An Empirical Model for the Ignition of Explosively Dispersed Aluminum Particle Clouds, Shock Waves **22**, 591 (2012).

[17] V. M. Boiko and S. V. Poplavski, Self-Ignition and Ignition of Aluminum Powders in Shock Waves, Shock Waves **11**, 289 (2002).

[18] A. L. Kuhl and V. M. Boiko, Ignition of Aluminum Particles and Clouds No. LLNL-CONF-427973. Lawrence Livermore National Lab.(LLNL), Livermore, CA (United States), 2010.

[19] V. M. Boiko, V. V. Lotov, and A. N. Papyrin, Ignition of Gas Suspensions of Metallic Powders in Reflected Shock Waves, Combust. Explos. Shock Waves **25**, 193 (1989).

[20] F. Zhang, S. B. Murray, and K. B. Gerrard, Aluminum Particles–Air Detonation at Elevated Pressures, Shock Waves **15**, 313 (2006).

[21] J. B. Middlebrooks, C. G. Avgoustopoulos, W. J. Black, R. C. Allen, and J. A. McFarland, Droplet and Multiphase Effects in a Shock-Driven Hydrodynamic Instability with Reshock, Exp. Fluids **59**, 98 (2018).

[22] D.-W. Vasco, A. Roy, W. C. Maxon, and J. A. McFarland, A Method for Measuring Droplet Evaporation in a Shock-Driven Multiphase Instability, Int. J. Multiph. Flow 103464 (2020).

[23] S. Gallier, F. Sibe, and O. Orlandi, Combustion Response of an Aluminum Droplet Burning in Air, Proc. Combust. Inst. **33**, 1949 (2011).

[24] M. W. Beckstead, Y. Liang, and K. V. Pudduppakkam, Numerical Simulation of Single Aluminum Particle Combustion (Review), Combust Explos Shock Waves **41**, 622 (2005).

[25] R. W. Houim, Modeling the Influence of Shock Waves on the Combustion of Aluminum Droplets, Ph. D. thesis, The Pennsylvania State University, 2011.

[26] P. Das and H. S. Udaykumar, Sharp-Interface Calculations of the Vaporization Rate of Reacting Aluminum Droplets in Shocked Flows, Int. J. Multiph. Flow 103442 (2020).

[27] K. Balakrishnan and S. Menon, On Turbulent Chemical Explosions into Dilute Aluminum Particle Clouds, Combust. Theory Model. **14**, 583 (2010).

[28] Z. J. Zhang, C. Y. Wen, Y. F. Liu, D. L. Zhang, and Z. L. Jiang, Effects of Different Particle Size Distributions on Aluminum Particle–Air Detonation, AIAA J. **58**, 3115 (2020).

[29] R. W. Houim and E. S. Oran, A Multiphase Model for Compressible Granular–Gaseous Flows: Formulation and Initial Tests, J. of Fluid Mech. **789**, 166 (2016).

[30] B. Shotorban, G. B. Jacobs, O. Ortiz, and Q. Truong, An Eulerian Model for Particles Nonisothermally Carried by a Compressible Fluid, Int. J. Heat Mass Transf. **65**, 845 (2013).

[31] G. B. Jacobs, W. S. Don, and T. Dittmann, High-Order Resolution Eulerian–Lagrangian Simulations of Particle Dispersion in the Accelerated Flow behind a Moving Shock, Theor. Comput. Fluid Dyn. **26**, 37 (2012).

[32] G. B. Jacobs and W.-S. Don, A High-Order WENO-Z Finite Difference Based Particle-Source-in-Cell Method for Computation of Particle-Laden Flows with Shocks, J. Comput. Phys. **228**, 1365 (2009).

[33] J. Glorian, S. Gallier, and L. Catoire, On the Role of Heterogeneous Reactions in Aluminum Combustion, Combust. Flame **168**, 378 (2016).

[34] S. E. Olsen and M. W. Beckstead, Burn Time Measurements of Single Aluminum Particles in Steam and CO2 Mixtures, J. Propuls. Power(2012).

[35] R. W. Houim and K. K. Kuo, A Ghost Fluid Method for Compressible Reacting Flows with Phase Change, J. Comput. Phys. **235**, 865 (2013).

[36] P. Das and H. S. Udaykumar, A Sharp-Interface Method for the Simulation of Shock-Induced Vaporization of Droplets, J. Comput. Phys. **405**, 109005 (2020).

[37] P. Das and H. S. Udaykumar, A Simulation-Derived Surrogate Model for the Vaporization Rate of Aluminum Droplets Heated by a Passing Shock Wave, Int. J. Multiph. Flow 103299 (2020).

[38] P. Lynch, H. Krier, and N. Glumac, A Correlation for Burn Time of Aluminum Particles in the Transition Regime, Proc. Combust. Inst. **32**, 1887 (2009).

[39] S. R. Gollahalli and T. A. Brzustowski, Experimental Studies on the Flame Structure in the Wake of a Burning Droplet, Symp. (Int.) on Combust. **14**, 1333 (1973).

[40] D. B. Spalding, The Combustion of Liquid Fuels, Symp. (Int.) on Combust. **4**, 847 (1953).

[41] T. L. Jiang, W. S. Chen, M. J. Tsai, and H. H. Chiu, A Numerical Investigation of Multiple Flame Configurations in Convective Droplet Gasification, Combust. Flame **103**, 221 (1995).

[42] M. Nakamura, F. Akamatsu, R. Kurose, and M. Katsuki, Combustion Mechanism of Liquid Fuel Spray in a Gaseous Flame, Phys. Fluids **17**, 123301 (2005).

[43] B. A. Khasainov and B. Veyssiere, Steady, Plane, Double-Front Detonations in Gaseous Detonable Mixtures Containing a Suspension of Aluminum Particles, Prog. Astronaut. Aeronaut.Prog. Astronaut. Aeronaut. **114**, 284 (1988).

[44] B. A. Khasainov, Model of Non-Premixed Combustion of Aluminium—Air Mixtures, in AIP Conference Proceedings, Vol. 845 (AIP, Baltimore, Maryland (USA), 2006), pp. 449–452.

[45] G. Wu and W. A. Sirignano, Transient Convective Burning of Interactive Fuel Droplets in Double-Layer Arrays, Combust. Flame **158**, 2395 (2011).

[46] B. Wang, A. Kronenburg, G. L. Tufano, and O. T. Stein, Fully Resolved DNS of Droplet Array Combustion in Turbulent Convective Flows and Modelling for Mixing Fields in Inter-Droplet Space, Combust. Flame **189**, 347 (2018).

[47] J. Shinjo, J. Xia, L. C. Ganippa, and A. Megaritis, Puffing-Enhanced Fuel/Air Mixing of an Evaporating -Decane/Ethanol Emulsion Droplet and a Droplet Group under Convective Heating, J. of Fluid Mech. **793**, 444 (2016).

[48] M. W. Beckstead, A summary of aluminum combustion. Brigham Young Univ Provo Ut, 2004.

[49] M. K. King, Aluminum Combustion in a Solid Rocket Motor Environment, Proc. Combust. Inst. **32**, 2107 (2009).

[50] M. Sussman, P. Smereka, and S. Osher, A Level Set Approach for Computing Solutions to Incompressible Two-Phase Flow, J. Comput. Phys. **114**, 146 (1994).

[51] H. S. Udaykumar and S. K. Sambasivan, Ghost Fluid Method for Strong Shock Interactions Part 1: Fluid-Fluid Interfaces, AIAA J. **47**, 2907 (2009).

[52] H. S. Udaykumar and S. K. Sambasivan, A Sharp Interface Method for High-Speed Multi-Material Flows: Strong Shocks and Arbitrary Materialpairs, Int. J. Comput. Fluid D. **25**, 139 (2011).

[53] P. Das, O. Sen, G. Jacobs, and H. S. Udaykumar, A Sharp Interface Cartesian Grid Method for Viscous Simulation of Shocked Particle-Laden Flows, Int. J. Comput. Fluid D. **31**, 269 (2017).

[54] J. A. Sethian and P. Smereka, Level Set Methods for Fluid Interfaces, Annu. Rev. Fluid Mech. **35**, 341 (2003).

[55] R. W. Schrage, *A Theoretical Study of Interphase Mass* Transfer (Columbia University Press, New York, NY, 1953).

[56] Y. Huang, G. A. Risha, V. Yang, and R. A. Yetter, Effect of Particle Size on Combustion of Aluminum Particle Dust in Air, Combust. Flame **156**, 5 (2009).

[57] See Supplemental Material at [URL Will Be Inserted by Publisher] for the numerical framework used in this work. Further details of the numerical methods and physical models used in the current calculations can be found in [36], [82]-[98].

[58] C. T. Crowe, J. D. Schwarzkopf, M. Sommerfeld, and Y. Tsuji, *Multiphase Flows with Droplets and Particles* (CRC Press, 2011).

[59] D. Igra and K. Takayama, Numerical Simulation of Shock Wave Interaction with a Water Column, Shock Waves **11**, 219 (2001).

[60] H. Terashima and G. Tryggvason, A Front-Tracking/Ghost-Fluid Method for Fluid Interfaces in Compressible Flows, J. Comput. Phys. **228**, 4012 (2009).

[61] M. Sun, T. Saito, K. Takayama, and H. Tanno, Unsteady Drag on a Sphere by Shock Wave Loading, Shock Waves **14**, 3 (2005).

[62] S. Sembian, M. Liverts, N. Tillmark, and N. Apazidis, Plane Shock Wave Interaction with a Cylindrical Water Column, Phys. Fluids **28**, 056102 (2016).

[63] Y. Mehta, C. Neal, T. L. Jackson, S. Balachandar, and S. Thakur, Shock Interaction with Three-Dimensional Face Centered Cubic Array of Particles, Phys. Rev. Fluids **1**, 054202 (2016).

[64] P. Das, O. Sen, G. Jacobs, and H. S. Udaykumar, Metamodels for Interphase Heat Transfer from Mesoscale Simulations of Shock–Cylinder Interactions, AIAA J. **56**, 3975 (2018).

[65] P. Das, O. Sen, K. K. Choi, G. Jacobs, and H. S. Udaykumar, Strategies for Efficient Machine Learning of Surrogate Drag Models from Three-Dimensional Mesoscale Computations of Shocked Particulate Flows, Int. J. Multiph. Flow **108**, 51 (2018).

[66] M. Jelezniak and L. Jelezniak, Chemked–A Program for Chemical Kinetics of Gas-Phase Reactions, (2013).

[67] D. Igra and K. Takayama, Investigation of Aerodynamic Breakup of a Cylindrical Water Droplet, Reports of the Institute of Fluid Science, Tohoku University **11**, 123 (2001).

[68] J. C. Meng and T. Colonius, Numerical Simulations of the Early Stages of High-Speed Droplet Breakup, Shock Waves **25**, 399 (2015).

[69] B. W. Weber and K. E. Niemeyer, ChemKED: A Human- and Machine-Readable Data Standard for Chemical Kinetics Experiments, Int. J. Chem. Kinet. **50**, 135 (2018).

[70] R. W. Houim and K. K. Kuo, A Low-Dissipation and Time-Accurate Method for Compressible Multi-Component Flow with Variable Specific Heat Ratios, J. Comput. Phys. **230**, 8527 (2011).

[71] I. Glassman, Metal combustion processes. Princeton Univ NJ James Forrestal Research Center, 1959.

[72] T. Bazyn, H. Krier, and N. Glumac, Oxidizer and Pressure Effects on the Combustion of 10-Micron Aluminum Particles, J. Propuls. Power**21**, 577 (2005).

[73] T. Bazyn, H. Krier, and N. Glumac, Combustion of Nanoaluminum at Elevated Pressure and Temperature behind Reflected Shock Waves, Combust. Flame **145**, 703 (2006).

[74] E. B. Washburn, J. A. Webb, and M. W. Beckstead, The Simulation of the Combustion of Micrometer-Sized Aluminum Particles with Oxygen and Carbon Dioxide, Combust. Flame **157**, 540 (2010).

[75] E. B. Washburn, J. N. Trivedi, L. Catoire, and M. W. Beckstead, The Simulation of the Combustion of Micrometer-Sized Aluminum Particles with Steam, Combust. Sci. Technol. **180**, 1502 (2008).

[76] O. Sen, N. J. Gaul, K. K. Choi, G. Jacobs, and H. S. Udaykumar, Evaluation of Multifidelity Surrogate Modeling Techniques to Construct Closure Laws for Drag in Shock–Particle Interactions, J. Comput. Phys. **371**, 434 (2018).

[77] O. Sen, N. J. Gaul, K. K. Choi, G. Jacobs, and H. S. Udaykumar, Evaluation of Kriging Based Surrogate Models Constructed from Mesoscale Computations of Shock Interaction with Particles, J. Comput. Phys. **336**, 235 (2017).

[78] O. Sen, S. Davis, G. Jacobs, and H. S. Udaykumar, Evaluation of Convergence Behavior of Metamodeling Techniques for Bridging Scales in Multi-Scale Multimaterial Simulation, J. Comput. Phys. **294**, 585 (2015).

[79] S. Roy, O. Sen, N. K. Rai, M. Moon, E. Welle, C. Molek, K. K. Choi, and H. S. Udaykumar, Structure–Property–Performance Linkages for Heterogenous Energetic Materials through Multi-Scale Modeling, Multiscale and Multidiscip. Model. Exp. and Des. **3**, 4 (2020).

[80] Z. Hosseinzadeh-Nik, S. Subramaniam, and J. D. Regele, Investigation and Quantification of Flow Unsteadiness in Shock-Particle Cloud Interaction, Int. J. Multiph. Flow **101**, 186 (2018).

[81] Y. Mehta, C. Neal, K. Salari, T. L. Jackson, S. Balachandar, and S. Thakur, Propagation of a Strong Shock over a Random Bed of Spherical Particles, J. of Fluid Mech. **839**, 157 (2018).

[82] T. P. Coffee and J. M. Heimerl, Transport Algorithms for Premixed, Laminar Steady-State Flames, Combust. Flame **43**, 273 (1981).

[83] R. J. Kee, M. E. Coltrin, and P. Glarborg, *Chemically Reacting Flow: Theory and Practice* (Wiley, 2003).

[84] M. J. Assael, K. Kakosimos, R. M. Banish, J. Brillo, I. Egry, R. Brooks, P. N. Quested, K. C. Mills, A. Nagashima, Y. Sato, and W. A. Wakeham, Reference Data for the Density and Viscosity of Liquid Aluminum and Liquid Iron, J. Phys. Chem. Ref. Data **35**, 285 (2006).

[85] A. Burcat, Thermochemical Data for Combustion Calculations, in Combustion Chemistry (Springer, 1984), pp. 455–473.

[86] V. Recoules and J.-P. Crocombette, Ab Initio Determination of Electrical and Thermal Conductivity of Liquid Aluminum, Phys. Rev. B **72**, 104202 (2005).

[87] J. Mousel, A Massively Parallel Adaptive Sharp Interface Solver with Application to Mechanical Heart Valve Simulations, Ph. D. thesis, The University of Iowa,2012.

[88] R. Scardovelli and S. Zaleski, Analytical Relations Connecting Linear Interfaces and Volume Fractions in Rectangular Grids, J. Comput. Phys. **164**, 228 (2000).

[89] G. R. Gathers, Thermophysical Properties of Liquid Copper and Aluminum, Int. J. Thermophys. **4**, 209 (1983).

[90] V. Sarou-Kanian, F. Millot, and J. C. Rifflet, Surface Tension and Density of Oxygen-Free Liquid Aluminum at High Temperature, Int. J. Thermophys. **24**, 277 (2003).

[91] S. Osher and J. A. Sethian, Fronts Propagating with Curvature-Dependent Speed: Algorithms Based on Hamilton-Jacobi Formulations, J. Comput. Phys. **79**, 12 (1988).

[92] G.-S. Jiang and C.-W. Shu, Efficient Implementation of Weighted ENO Schemes, J. Comput. Phys. **126**, 202 (1996).

[93] S. Gottlieb and C.-W. Shu, Total Variation Diminishing Runge-Kutta Schemes, Math. Comp. **67**, 73 (1998).

[94] R. R. Nourgaliev, S. Wiri, N. T. Dinh, and T. G. Theofanous, On Improving Mass Conservation of Level Set by Reducing Spatial Discretization Errors, Int. J. Multiph. Flow **31**, 1329 (2005).

[95] J. G. Verwer, B. P. Sommeijer, and W. Hundsdorfer, RKC Time-Stepping for Advection–Diffusion–Reaction Problems, J. Comput. Phys. **201**, 61 (2004).

[96] P. N. Brown, G. D. Byrne, and A. C. Hindmarsh, VODE: A Variable-Coefficient ODE Solver, SIAM J. Sci. and Stat. Comput. **10**, 1038 (1989).

[97] C.-W. Shu and S. Osher, Efficient Implementation of Essentially Non-Oscillatory Shock-Capturing Schemes, II, J. Comput. Phys. **83**, 32 (1989).

[98] S. K. Sambasivan and H. S. UdayKumar, Ghost Fluid Method for Strong Shock Interactions Part 1: Fluid-Fluid Interfaces, AIAA J. **47**, 2907 (2009).